A MULTI-SCALE STUDY OF THALAMIC STATE-DEPENDENT RESPONSIVENESS

JORIN OVERWIENING (1,2), FEDERICO TESLER (1), DOMENICO GUARINO (1) and ALAIN DESTEXHE (1)

(1)
Department for Integrative and Computational Neuroscience (ICN), Paris-Saclay Institute of Neuroscience (NeuroPSI), Campus CEA Saclay,
151 route de la Rotonde, Bâtiment 151, Saclay, 91400, France

(2)
Institute for Theoretical Physics (ITP), University of Muenster,
Wilhelmsstraße 11, Münster, 48147, Germany

Contact: JORIN OVERWIENING
overwiening@uni-muenster.de

ABSTRACT

The thalamus is the brain's central relay station, orchestrating sensory processing and cognitive functions. However, how thalamic function depends on internal and external states, is not well understood. A comprehensive understanding would necessitate the integration of single cell dynamics with their collective behaviour at population level. For this we propose a biologically realistic mean-field model of the thalamus, describing the dynamics of thalamocortical relay neurons (TC) and thalamic reticular neurons (RE). With this we perform a multi-scale study of thalamic responsiveness and its dependence on cell, synaptic, and brain states. Based on existing single-cell experiments we show that: The transition between tonic and burst states of TC cells acts as a linear-nonlinear switch in the thalamic response to stimuli. In the awake state, sensory stimuli generate a linear thalamic response while cortical input to the thalamus generates a nonlinear response. And that stimulus response and information transfer are controlled by cortical input and synaptic noise, which both suppress responsiveness. In addition, synaptic noise acts as an equalizer between thalamic response at different states and diffuses state transitions between tonic-bursting and awake-sleep states. Finally, the model replicates spindles within a sleep-like state, reducing its responsiveness. This study results in new insight on the brain-state dependent function of the thalamus. In addition, the development of a novel thalamic mean-field model provides a new a tool for incorporating detailed thalamic dynamics in large scale brain simulations. This will help to bridge the gap between computational neuroscience, behavioral experiments, and the study of brain diseases.

INTRODUCTION

The thalamus, a well preserved structure found in mammals (Rose and Woolsey, 1949), serves as a crucial relay station in the central nervous system. Diverse thalamic nuclei function as transmitters of sensory information from the periphery to the cortex and other central nervous system structures, while also facilitating the transfer of motor commands from the cortex to various regions of the body (Kandel, Schwartz, and Jessell, 1991, ch. 15-16). Each of the relatively independent thalamic nuclei comprises at least two cell types: excitatory principal *relay* cells, featuring extensive axonal projections to various nervous system structures, but rarely to other principal cells, and local interneurons (Sherman and Koch, 2004; Jones, 1985).

The primary source of activity in thalamic nuclei arises from direct pathways, operating in both peripheral-to-central and central-to-peripheral directions. During wakefulness, thalamic relay neurons display tonic firing. However, neuromodulators like acetylcholine (ACh) or hyperpolarizing inputs can introduce complex dynamics, including bursting and rebound bursts (Sherman and Guillery, 2009). Additionally, cortical feedback projections exert a strong influence on the thalamus. Notably, the number of thalamo-cortical outgoing axons is approximately one-tenth of the number of cortico-thalamic incoming axons (Pinault and Deschênes, 1998; Sherman and Koch, 2004), and the cortex is the major source of synapses within the thalamus, for example accounting for 50% of synapses in the lateral geniculate nucleus Sherman and Koch, 2004). This extensive feedback loop between the thalamus and cortex indicates a substantial role of the cortex in thalamic relay functions (Crandall, Cruikshank, and Connors, 2015).

Surrounding the thalamus, the thalamic reticular nucleus (TRN) contains GABAergic reticular cells (RE) that broadly inhibit thalamic nuclei, and themselves through nets of axonal and dendritic connections (Sherman and Koch, 2004; Sherman and Guillery, 2009). RE neurons can be activated through feedforward signals from thalamic nuclei or feedback from the cortex. These neurons consistently exhibit bursting behavior and can induce similar patterns in thalamic relay cells via hyperpolarization. This recurrent network allows the cortex and thalamus to actively regulate its information flow, rendering it as a gate, with the TRN serving as its gatekeeper.

In addition to its gating function, there is also evidence of the thalamus playing a role in creating whole brain dynamics such as spindle and delta oscillations and supporting or controlling them–for instance, during slow waves in non-REM sleep or anaesthesia (see Brown et al., 2012; Gent et al., 2018; Schreiner et al., 2022). It is suggested that the intrinsic loop between thalamocortical (TC) relay and RE cells plays a pivotal role in all of these behaviours by acting as a pacemaker and oscillator. The crucial mechanism at play is the rebound bursting of relay cells induced by RE inhibition, which depends on the state and polarization of the relay cells.

These oscillatory behaviors primarily manifest during sleep-like brain states, where the firing mode of TC relay cells differs significantly from that observed during wakefulness, with an increased prevalence of bursting (Ramcharan, Gnadt, and Sherman, 2000). Moreover, integration with cortical pathways suggests the thalamus plays a role in higher brain functions, encompassing sensation, attention, and arousal (Wimmer et al., 2015; Mitchell et al., 2014).

Investigating the interaction between thalamic reticular and relay neurons at various levels is crucial for deciphering the mechanics of sensation, attention, arousal, sleep and cognition. To this end it is necessary to analyse such neuron interactions and their corresponding population activity via large-scale models. One feasible approach for scaling upwards is to employ interconnected single-cell neuron models, but the computational demand rapidly increases as the network size is taken to the scale of even the smallest anatomical subdivisions of the brain. For larger scales and even whole-brain simulations, it is necessary to decrease computational complexity. This can be achieved by reducing the degrees of freedom and describing populations of neurons as the smallest units. A viable option is to use a mean-field theory to model population dynamic statistics, such as firing rate.

Most existing neuronal field models can be separated in two groups: either phenomenological models (e.g. Sanz-Leon et al., 2015; Breakspear, 2017; Bassett, Zurn, and Gold, 2018), or more abstract mathematical models (e.g. Amit, Gutfreund, and Sompolinsky, 1985; Coombes, 2005; Victor et al., 2011). Phenomenological models replicate biological behaviour and are capable of

modelling particular brain regions, cell types or whole brain recordings. However, these can not couple significant effects or characteristics with model parameters which makes it impractical to use such models far of the fitting point and renders analytical analysis unuseful. Conversely, mathematical models include all nonlinear dynamics and provide tools to analyse states and dynamics, but these behaviours are often not well linked to biological observables.

To strike a good balance between these two options, we follow DiVolo et al. (2019) to create a *biologically realistic* mean-field model of the thalamus that also allows analytical analysis. To achieve this *biological realism* with an Adex based model, we shall proceed in two ways. Firstly, we find realistic thalamic single-cell behaviour producing parameters and then construct the mean field bottom-up in an semi-analytical way, validating it with experiments across all scales. Secondly, the approach incorporates three crucial biological features: First, *irregular spiking* activity of single neurons is believed to be important for transfer efficiency (Doron et al., 2014) and the correct baseline for neurons in both awake-like asynchronous states (Bellay et al., 2015) as well as in sleep-like synchronous states (Steriade, Timofeev, and Grenier, 2001). The term used to describe the standard activity state is therefore referred to as *asynchronous irregular* (AI). Second, *conductances* are a crucial nonlinearity to incorporate in modelling. In contrast to current-based systems, they can demonstrate diverse states in response to the same stimulus and encompass biological synaptic properties into the model. Moreover, Vogels and Abbott (2005) showed that using conductance-based models leads to self-sustained activity. And last, *adaptation* mechanics in respect to spiking rate and membrane potential are the main generators of bursting behaviour and crucial for achieving realistic firing rate saturation such as with *regular spiking* cells in the cortex.

At the core of this mean-field formalism are the differential equations describing the mean and higher order statistical moments of spiking networks from El Boustani and Destexhe (2009). This formalism requires an already known analytical transfer function for each neuron type. In Zerlaut et al. (2016) a semi-analytical approach was developed to fit the transfer function to single cell data. This enables the use of experimental data or acquiring a numerical transfer function for neurons based on single-cell neuronal models. In particular we will consider here the *Adaptive exponential integrate and fire model* (Adex) (see Brette and Gerstner, 2005; Touboul and Brette, 2008). The Adex captures the above mentioned critical features at single cell level and shows all realistic firing modes as observable in real cells (Izhikevich, 2004). Furthermore, this model can also precisely emulate the behaviour of cells in the thalamo-cortical system (Destexhe, 2009).

In this study, we investigate the state-dependent responsiveness of the thalamus. For this we build a biologically realistic spiking network and mean-field model, incorporating thalamic structure. Based on existing single-cell experiments we show that: First, the transition from tonic to burst firing of TC cells renders thalamic response nonlinear. Second, sensory stimuli generate linear response, while cortical inputs generate nonlinear response. Third, that cortical input and noise suppress thalamic response at all scales and that noise diffuses thalamic state transitions. Finally, we demonstrate that the proposed models are capable of generating self-sustained spindle oscillations in a sleep-like state, in which responsiveness is reduced.

METHODS

In this section we describe the spiking and the mean-field model. The chosen network and connectivity structure as well as cell and synaptic parameters are derived and motivated.

Spiking model

Here we employ spiking simulations based on the *Adaptive exponential integrate and fire model* (Adex) (as defined in Brette and Gerstner, 2005). This conductance based model numerously proved to be a good balance between computability and biological realism in terms of capturing all firing modes observable in real cells (see Izhikevich, 2004) and significantly in thalamocortical

cells (Destexhe, 2009). The dynamical system is the two equations describing membrane potential v and adaptation ω of a given cell μ

$$c_m \frac{\mathrm{d}v_\mu}{\mathrm{d}t} = g_L(E_L - v_\mu) + g_L \Delta \, \mathrm{e}^{\frac{v_\mu - V_t}{\Delta}} - \omega_\mu + I_{\mathrm{syn}}(t) \tag{1}$$

$$\frac{\mathrm{d}\omega_\mu}{\mathrm{d}t} = -\frac{\omega_\mu}{\tau_\omega} + b \sum_{t_s} \delta(t - t_s) + a(v_\mu - E_L), \tag{2}$$

where the cell parameters are listed in Table 1 and I_{syn} is an input modeling all incoming synaptic currents. It consists of an excitatory and inhibitory current each equal to the cells potential and spike dependent synaptical conductances G_{syn}

$$I_{\mathrm{syn}}(t) = (E_e - v_\mu) G^e_{\mathrm{syn}}(t) + (E_i - v_\mu) G^i_{\mathrm{syn}}(t) \tag{3}$$

$$G^{(e,i)}_{\mathrm{syn}}(t) = Q_{(e,i)} \sum_{t_s^{(e,i)}} \theta(t - t_s^{(e,i)}) \, \mathrm{e}^{-\frac{t - t_s^{(e,i)}}{\tau_{(e,i)}}}, \tag{4}$$

where G_{syn} is modeled such that each time a spike (t_s) arrives these conductances experience an increment Q and exponentially relax again with time constant τ.

Additional to the integration of this ODE set comes the usual spike mechanism employed in integrate and fire models: A spike of neuron μ is counted if $v_\mu > V_{\mathrm{thr}} = -20\mathrm{mV}$, then the membrane potential is reset to $V_r = \{-55\mathrm{mV}$ for RE, $-50\mathrm{mV}$ for TC$\}$ for a refractory period of 5ms, and the adaptation current ω experiences an increment of b.

Architecture and parameters

We model one thalamocortical relay (TC) and one connected reticular (RE) population of a generic thalamic nucleus. We neglect interneurons, as we assume to be in the limit of large and sparsely connected networks. Then, their correlations become insubstantial and interneurons are not contributing to population dynamics (Steriade, Deschênes, et al., 1985). One of the main goals of the thalamus mean-field is to be incorporated into large or whole brain models with, among others, already developed cortical mean-field models (DiVolo et al., 2019). These describe populations of $\sim 10^4$ cortical neurons. To keep the scale difference between cortex and thalamus proportional, we employ a scale of 1/10 (Pinault and Deschênes, 1998; Sherman and Koch, 2004) and therefore use $N = 500$ neurons per population.

The network with its connections is depicted in Figure 1a. We consider a random connected *Erdős-Rényi* network comparable to the statistical assumptions of the mean-field. TC and RE populations form a loop of excitation and inhibition. TC cells do not excite other TC cells but RE cells (next to outgoing axons to the cortex). In contrast, RE are connected in an inhibitory loop and also inhibit TC cells. We propose two external drives serving as inputs to the model: The *cortical* drive P (going to both populations) and the *sensory* drive S (going only to TC cells) modeling cortical signals and sensory stimuli to the thalamus, respectively.

For the synaptic and connection parameter values, we start with a connection between populations of 5% and increments of $Q_e = 1\mathrm{nS}$ to be close to the values of previous mean-field models (e.g. DiVolo et al., 2019) and we change from there to incorporate biological structures:

To model the dense net of locally self-inhibiting RE neurons in the TRN (refer e.g. Lee et al., 2014; Kandel, Schwartz, and Jessell, 1991), we use a high $p = 30\%$ and a balancing low $Q = 1\mathrm{nS}$. According to studies such like Sherman and Koch (2004) and Sherman and Guillery (2009) there are significant more axons going from cortex to TC than from cortex to RE cells, but the amplitude of connection are stronger, keeping the impactfulness of the role of TRN in the cortico-thalamic control. Last, the number and convergence of connections from RE to TC cells ensure strong inhibition (Sherman and Guillery, 2009).

Moving to cell parameters, we model two states of the thalamus corresponding to either an absence of the excitatory modulator acetylcholine (ACh) or its presence. In McCormick and Prince (1986), it was shown that ACh changes the firing patterns of RE cells to inhibit single tonic firing of TC cells and to promote bursting. Because of the capability of ACh to act as a

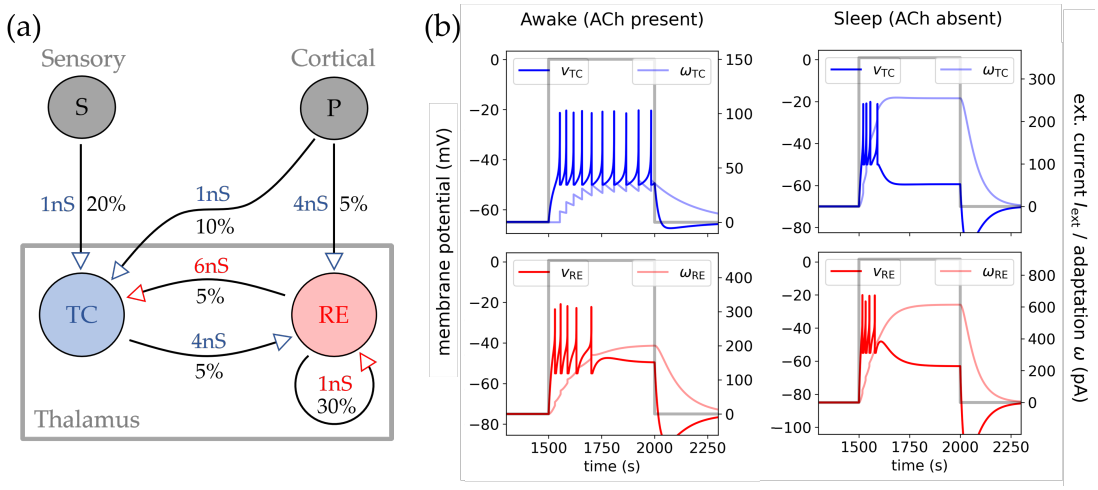

Figure 1: Network structure and single cell dynamics. (a) The chosen network structure of two thalamic populations (TC and RE cells of each $N = 500$), their synaptic increments Q, and connection probabilities p for all connection between the TC and RE population. The external inputs are shown in grey: The *cortical* drive P ($N = 8000$) and the *sensory* stimulus drive S ($N = 500$). The arrows mark the direction of synaptic transmission and if they act excitatory (blue) or inhibitory (red). **(b)** Single cell traces from Adex IF neurons (see Methods for details) of TC and RE for a timed constant input current (grey line). The left column shows TC and RE response to the injected current in awake state (with ACh) and the right column the same in sleep state (no ACh). The cells membrane potential v and adaptation current ω are shown in color for TC (blue) and RE cell (red), respectively.

switch between tonic and bursting mode in the TC cells relay, and its role in controlling the overall brain state (Castro-Alamancos and Connors, 1996; McCormick, McGinley, and Salkoff, 2015; Steriade, Deschênes, et al., 1985), we define here these two states as *awake* state (ACh present) and *sleep* state (ACh absent).

We will follow the approach from a preceding study (Guarino and Destexhe, 2023) to analyse the parameter space and choose realistic cell parameters. The parameter values are based on the values proposed in Destexhe (2009) with taking into account experimentally evident ranges (see Guarino and Destexhe, 2023 for details). The Adex (1) was fitted on recorded cell traces of TC and RE neurons with and without ACh present from McCormick and Prince (1986). The resulting parameters are shown in Table 1 and their fit is validated on the whole parameter space in Figure 7–Figure 10. The most critical difference to Guarino and Destexhe (2023) lies in a hyperpolarised E_L for RE cells in sleep state. This choice does deviate from a best fit as is evident from the high error as shown in the second row in Figure 9. However, this was necessary to guarantee biologically realistic stable and inhibition controlled AI dynamics of the full network.

To show that the cells inherit the correct behaviour, using the Adex (1) with the proposed cell parameters, in Figure 1b four exemplary single cell traces of RE and TC are shown. In there a constant–time gated–current was injected in to the cell to invoke a firing response of the cell. This was done by setting a rectangular pulse as I_{syn} in (1). In earlier works (see Wang, Li, and Wu, 2021) it was shown that such a synaptic current serves as the bifurcation parameter evoking either bursting via a *homo-clinic* bifurcation or tonic firing via a *saddle-node Hopf* bifurcation. The top row, using the awake parameters (including the modulatory effect of ACh), shows the wanted responses: being tonic firing for the TC cell and bursting for the RE cell. In the bottom row the parameters for sleep (excluding the effect of ACh) change the tonic mode of TC into bursting behaviour and keep the bursting of the RE cells, albeit increasing its *burstiness*.

Table 1: Used cell and synaptic parameters for TC and RE cells in awake (ACh) and sleep (no ACh) states, respectively. The last two parameters are for the spiking network only.

	AWAKE		SLEEP		
PARAM	TC	RE	TC	RE	DESCRIPTION
Q_e	1nS	4nS	-	-	exc.quant. conductance increment
Q_i	6nS	1nS	-	-	inh.quant. conductance increment
c_m	160pF	200pF	-	-	membrane capacitance
E_L	-65mV	-75mV	-70mV	-85mV	resting (leakage) potential
g_L	10nS	10nS	9.5nS	13nS	leak conductance
τ_w	200ms	200ms	270ms	230ms	adaptation time const.
a	0nS	8nS	24nS	28nS	membrane potential adaptation
b	10pA	10pA	20pA	20pA	spike frequency adaptation
$\tau_{(e,i)}$	5ms	5ms	-	-	syn. time constants
E_e	0mV	0mV	-	-	exc. reversal potential
E_i	-80mV	-80mV	-	-	inh. reversal potential
V_t	-50mV	-45mV	-	-	threshold for the exp. onset
Δ	4.5mV	2.5mV	-	-	amplitude of the spike onset

Mean-field model

El Boustani and Destexhe (2009) developed a second-order mean-field formalism of ordinary differential equations describing the firing rate statistical moments of spiking networks. This general framework is applicable to any arbitrary neuron models as long as a characteristic transfer function can be defined. It is assumed that the network is (sparsely) randomly connected and balanced (*Erdős-Rényi model*). It is derived with the assumption of the system being in AI state. This is improved by adding the slow dynamic effects of adaptation (DiVolo et al., 2019), then the ODE system reads:

$$T\frac{\partial \nu_\mu}{\partial t} = (F_\mu - \nu_\mu) + \frac{1}{2}\partial_\lambda \partial_\eta F_\mu c_{\lambda\eta} \tag{5}$$

$$T\frac{\partial_t c_{\mu\nu}}{\partial t} = \delta_{\mu\nu} A^{-1}_{\mu\mu} + (F_\mu - \nu_\mu)(F_\nu - \nu_\nu) + \partial_\lambda F_\mu c_{\nu\lambda} + \partial_\lambda F_\nu c_{\mu\lambda} - 2c_{\mu\nu} \tag{6}$$

$$\partial_t W_\mu = -\frac{W_\mu}{\tau_\omega} + b\nu_\mu + a((\mu_V)_\mu - E_L), \tag{7}$$

where ν is the mean firing rate, F the transfer function, c the correlation, and W the adaptation of a given cell population μ. The indices $\{\mu, \nu, \lambda, \eta\}$ run over the set of populations, e.g. in our case of two populations the set of $\{e, i\}$ for excitatory TC and inhibitory RE. The derivatives are defined as $\partial_\mu = \frac{\partial}{\partial \nu_\mu}$. Important to note is the role of T which marks the upper limit where all dynamics with smaller time resolutions are not captured.

The core of this formalism is the transfer function and so the main task in constructing a mean-field of the thalamus is to get the transfer function of TC and RE cells in the two states we are interested in. For simple neuron models the transfer function can be derived purely analytically, this however is not the case for the highly nonlinear Adex model.

To derive the transfer function we therefore follow the approach of (Zerlaut et al., 2016), which is semi-analytic. In there the firing rate is written as a probabilistic function counting the spikes in term of the membrane potential ν being above a certain *spike threshold potential* V_{thr} in each time bin of duration τ_V which resembles the membrane potentials autocorrelation time. In the Gaussian limit we get a function dependent on the membrane subthreshold fluctuation statistical moments and define that as our transfer function:

$$F \equiv \nu_{\text{out}} = \frac{\text{prob}(v > V_{\text{thr}})}{\tau_V} \overset{\text{Gaussian}}{=} \frac{1}{2\tau_V}\text{erfc}\Big(\frac{V_{\text{thr}}^{\text{eff}} - \mu_V}{\sqrt{2}\sigma_V}\Big), \tag{8}$$

where μ_V is the mean and σ_V the standard deviation of the membrane potential (subthreshold). In the second step, the constant threshold V_{thr} is replaced with a phenomenological one acting as a function dependent on–and therefore accounting for–different cell properties. Because there is no theoretical form, a general second order polynomial dependent on the set $\{\mu_V, \sigma_V, \tau_V\}$ was proposed:

$$V_{\text{thr}}^{\text{eff}}(\mu_V, \sigma_V, \tau_V^N) = P_0 + \sum_{x \in \{\mu_V, \sigma_V, \tau_V^N\}} P_x \cdot \frac{x - x^0}{\delta x^0} + \sum_{x,y \in \{\mu_V, \sigma_V, \tau_V^N\}^2} P_{xy} \cdot \frac{x - x^0}{\delta x^0}\frac{y - y^0}{\delta y^0}, \tag{9}$$

where $\tau_V^N = \tau_V \frac{g_L}{c_m}$ is the non-dimensionalised autocorrelation and the parameters space is normalised to limit the fluctuation driven regime, with the mean x^0 and deviation δx^0.

Here either single cell simulations or experimental clamp data can be used to get values for the unknown amplitudes $\{P\}$. This fitting has to be done for each distinctive cell type, so in our case for TC and RE neurons. Because the two states awake and sleep are mostly changes in adaptation parameters, and it was shown in (DiVolo et al., 2019) that the mean-field is predictive even far from its fitting point, we just need one fit per cell type. This also is biologically realistic, for the changes induced by e.g. ACh would not change the cell morphology, and we consider the threshold membrane potential to stay the same for both states.

The set of $\{\mu_V, \sigma_V, \tau_V\}$ can be calculated purely analytically (see Kuhn, Aertsen, and Rotter, 2004) by using Campbell's theorem and assuming Poissonian distribution of incoming spikes as the generator of subthreshold fluctuations (as is the case with AI dynamics). The mean or static synaptic conductances are calculated then as a function of incoming spike frequencies $\{\nu_e, \nu_i\}$ in terms of their mean and standard deviation:

$$\mu_{G(e,i)} = \nu_{(e,i)} K_{(e,i)} \tau_{(e,i)} Q_{(e,i)} \tag{10}$$

$$\sigma_{G(e,i)} = \sqrt{\frac{\nu_{(e,i)} K_{(e,i)} \tau_{(e,i)}}{2}} Q_{(e,i)}, \tag{11}$$

where $K_\mu = pN_\mu$. With that the general input conductance of the cell can be computed

$$\mu_G(\nu_e, \nu_i) = \mu_{Ge} + \mu_{Gi} + g_L. \tag{12}$$

Using that we can calculate the mean membrane potential μ_V from the linear parts of (1) as a function of incoming spike frequencies

$$\mu_V(\nu_e, \nu_i, \omega) = \frac{\mu_{Ge} E_e + \mu_{Gi} E_i + g_L E_L - \omega}{\mu_G}. \tag{13}$$

Taking (3) as the general synaptic input, we can calculate the form of a single postsynaptic potential (PSP). And via shotnoise theory get the density power spectrum of membrane fluctuations $P_V(f)$ as a response to a stimulation (3). Then the variance of fluctuations with taking the integral $\sigma_V^2 = \int P_V \, \mathrm{d}f$, follows to

$$\sigma_V(\nu_e, \nu_i) = \sqrt{\sum_{(e,i)} K_{(e,i)} \nu_{(e,i)} \frac{(U_{(e,i)} \cdot \tau_{(e,i)})^2}{2(\tau_m + \tau_{(e,i)})}}, \tag{14}$$

where $\tau_m(\nu_e, \nu_i) = \frac{C_m}{\mu_G}$ and $U_{(e,i)} = \frac{Q_{(e,i)}}{\mu_G}(E_{(e,i)} - \mu_V)$.

Transfer function fit

To get the transfer functions we fit $\{P\}$ on single cell simulations of TC and RE cells (in awake state) using the Adex equations (1). The formalism translates excitatory and inhibitory input

firing rates $\{\nu_e, \nu_i\}$ of a neuron into its fluctuation statistics $\{\mu_V, \sigma_V, \tau_V\}$ and then to its output firing rate.

The advantage of this semi-analytic approach is that–given either simulated or experimental data–we can calculate the phenomenological threshold $V_{\text{thr}}^{\text{eff}}$ via reordering of (8). Then the employed procedure is to first fit (9) linearly in the threshold space (depending on the topography of the space to capture, this fit can be done nonlinearly too). However, here (13) has to be adjusted because the adaptation ω is unknown. Therefore, the (stationary) solution to (7) will be used to calculate ω from the firing rate data. The resulting values for $\{P\}$ are following used as initial guesses for the fully nonlinear fit of (8) in the original firing rate space.

For the fit we normalised the fluctuation regime the same way as done in previous works (Zerlaut et al., 2016 and DiVolo et al., 2019) to ensure comparability: $\mu_V^0 = -60$mV, $\delta\mu_V^0 = 10$mV, $\sigma_V^0 = 4$mV, $\delta\sigma_V^0 = 6$mV and $\tau_V^{N\,0} = 0.5$, $\delta\tau_V^{N\,0} = 1$.

Table 2: The fitting parameters of $V_{\text{thr}}^{\text{eff}}$ and their values. All values in mV.

cell	P_0	P_μ	P_σ	P_τ	$P_{\mu\mu}$	$P_{\mu\sigma}$	$P_{\mu\tau}$	$P_{\sigma\sigma}$	$P_{\sigma\tau}$	$P_{\tau\tau}$
TC	−47.31	1.68	0.97	−3.46	0.47	−1.68	−6.46	3.43	−1.14	0.19
RE	−40.77	−1.98	−3.12	3.57	1.39	−0.38	−0.33	0.16	0.26	−0.53

RESULTS

The results of this paper are structured as follow: First we will compare the mean-field model with simulated spiking network dynamics and proof its validity in and far of the fitting point. Then we will proceed to use the validated model and investigate the core functions of the thalamus. First, we focus on the thalamus' responsiveness and information transfer capabilities dependent on different external and internal states. We look at bursting and sleep-like states, and the controlling role of cortical inputs and synaptic noise. Lastly, thalamus specific spindle oscillations in a sleep-like state will be investigated.

Fitting and validation

In this section, we validate the mean-field model and demonstrate its suitability for modeling both awake and sleep states by comparing it with spiking networks.

The fit parameters of the mean-field's transfer function, obtained using the fitting technique described in the methods section, are depicted in Table 2. These parameters are applied to both awake and sleep states and are used throughout this and the following three sections (but not in the last one).

In Figure 2a, we show the fitted transfer functions for TC cells (top, blue) and RE cells (bottom, red) across the full range of excitatory input frequencies (ν_e) and a subset of three inhibitory input frequencies (ν_i). Each dot represents the mean output frequency from single-cell simulations over 5 seconds. The sigmoid shape of the transfer function (8) is evident. Deviations from mean-field predictions in single cell simulations can be attributed to the statistical nature of the system, which relies on Poissonian spike train inputs for (ν_e, ν_i). To improve statistics because of random Poissonian inputs, we averaged the resulting single-cell firing rates over 100 runs.

A direct validation of the mean-field model involves comparing the predicted mean firing rates and their standard deviations with those of the full spiking network, which models the entire thalamic substructure (Figure 1a). This comparison is shown in Figure 2c. Both populations receive an external constant *cortical* input of $P = 4$Hz and a double Gaussian stimulus coming from *sensory* input S (definition in appendix). The spiking network provides the membrane potential evolution and spiking times t_s for all cells. The spikes of all neurons are shown in the upper raster plot. By averaging $\{t_s\}$ over a specific bin time T_{bin}, we calculate the time-dependent mean firing rate of the spiking population. We use $T_{\text{bin}} = 5$ms for all

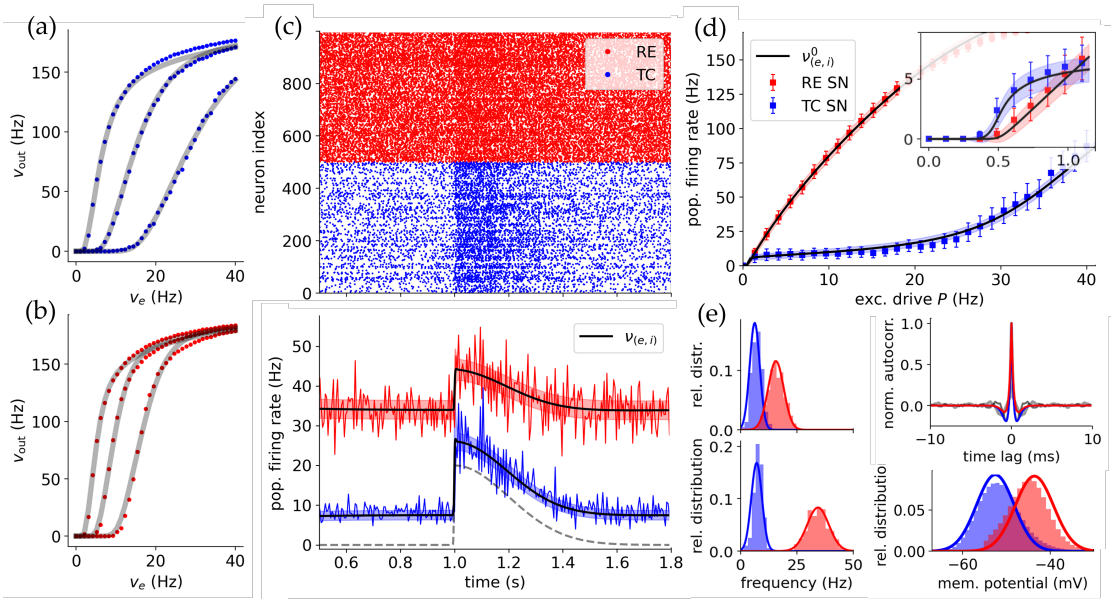

Figure 2: Validating the mean-field with spiking networks. (a,b) The fitted transfer functions for RE and TC cell for three different inhibitory inputs each with their corresponding single cell simulations. Top (a, blue) is for TC and bottom (b, red) for RE cell-type (in awake state). The dots each represent the averaged firing rate of a cell over 100 runs. **(c)** Comparison of the firing rate of the mean-field and the spiking network for constant cortical drive $P = 4$Hz and a Gaussian stimulus coming from S. Top is the raster plot showing all spiking times $\{t_s\}$ for all neurons in the spiking network simulation. Bottom is the averaged mean firing rate of spiking network (blue/red lines) and predicted mean firing rate of the mean-field ν (black line) with its standard deviation (shaded blue/red areas). **(d)** Comparison of the mean firing rate and corresponding standard deviation of the spiking network and the mean-field over a range of cortical inputs. Each dot represents a spiking network simulation for 10s where the steady long time mean is calculated. The black lines correspond to the mean-fields fixpoints $\nu^0_{(e,i)}$, with the shaded areas being the standard deviations. The inset shows a zoom at the *silent* and *inital* regimes (see main text for futher discussion). **(e)** Left column: The firing rate distributions of spiking network (histogram) and mean-field (line) for $P = \{2, 4\}$Hz. Bottom-right: Comparison of membrane potential distribution for 4Hz. Top-right: Autocorrelation of TC and RE population for spiking network (grey lines) and mean-field (blue/red lines).

simulations except stated otherwise. To compare to the mean-field, in the formalism we have to employ a similar or the same time window for the mean-fields time constant T, and we set $T = T_{\text{bin}}$. We see the network and mean-field show the wanted balanced excitation-inhibition state in AI regime with RE activity being dominant.

In Figure Figure 2d, we vary the cortical drive P and compare the equilibrium population firing rates (methodology in appendix) for TC and RE populations in both the spiking network and mean field over a 10-second simulation. This analysis reveals four distinct regimes of TC response: the first regime with no activity, the second regime with a fast response to changes in P, the inhibited third regime with limited responses and the fourth regime with strong TC cell responsiveness due to saturated RE cell activity. This justifies using a cortical drive $P > 1$Hz for most simulations, ensuring a stable low-activity AI state comparable to especially in-vivo experiments.

In Figure 2e, we compare the distribution of firing rates and membrane potentials. In the latter the refractory states are removed to get a realistic comparison with the mean-field. The good agreement in not only firing rate but also membrane potential is significant. (See Figure 12 for a discussion). Equations (13) and (14) predict accurately the spiking populations membrane potential and can henceforth be used to compare with experimental data and methods.

In the same figure, top-right there is also depicted a comparison of auto-correlations of TC and RE populations activity in the stationary state corresponding to $P = 4$Hz (see appendix

for the definition), showing a strong independence of population activity as expected from a inhibition-controlled network without excitatory-excitatory connections. This also agrees with the models being in AI state and the choice of T_{bin} and T for $\tau = 5$ms is justified.

Finally, we assess the robustness of the mean-field by varying global parameters (see Figure 11 in the appendix). This is done for adaptation parameters $\{b, a\}$, which exhibit significant change between awake and sleep state, and synaptic excitatory conductance Q_e, to validate its change in for simulations conducted later on in this study. We demonstrate that even far of the actual fitting point, the mean-field remains effective in capturing network dynamics. This validation allows us to use the mean-field approach for parameter space analysis and the study of the transition between awake and sleep states.

All this let us conclude that the mean-field works well in capturing the dynamics and activities of the spiking network while both show biologically realistic ranges and AI dynamics while being stable in an excitation-inhibition balance.

Bursting and Sleep

We explore how bursting (the state of ACh) impacts the response of individual neurons and of the population. Based on the fit to bursting TC cells from McCormick and Prince (1986) we can already state that the employed parameter set with the Adex shows bursting of single TC cells in the ACh depleted or sleep state (Figure 1). Following, we aim to replicate experiments at single cell level on tonic and bursting behaviors in TC cells, as documented in (Sherman and Guillery, 2009, ch. 6). These experiments involved manipulating the membrane potential of recorded cells to induce either tonic mode (around -65mV, resting state) or bursting mode (around -75mV, hyperpolarised state) in the absence of external stimuli. The stimulus applied in the experiment was a moving grating, leading to an oscillatory firing rate response. Tonic mode exhibited a linear response, while bursting mode showed responses primarily during the initial phase of each stimulus period.

We recreated exactly this behaviour in our proposed spiking network with an oscillatory sensory drive, with an amplitude of 50Hz and frequency of 2Hz. We set the network in awake state emulating the lightly anaesthetised state from experiment. To model thalamus in-vivo, a constant external cortical drive of $P = 4$Hz was applied (the *inhibited* regime). Subsequently, we recorded one single cell with each awake and sleep parameters. While our proposed awake and sleep states are not identical to the artificially set tonic and bursting modes in the experiment, the switch via acetylcholine (ACh) produces the same dynamics. We term our sleep state as analogous to the bursting mode in the experiment, with the only difference being in a change of adaptation parameters ($a = 10$nS and $b = 300$pA) required to match the shape of the experiment. These parameters are in line with the parameter scans (Figure 7–Figure 10) but adaptation now is stronger dependent on the cells spiking than on their membrane potential polarisation. The following simulations are done in sleep state with and without adjusted adaptation parameters.

The recorded cell's response was calculated by averaging the spike times over 40 simulations for a time bin of 15s. This firing rate is depicted in the first row of each Figure 3(a,b) for the awake state and sleep state state with and without adjusted adaptation parameters. We observe the same response patterns as in the experiment for awake and adjusted sleep parameters, although with slightly lower response amplitudes compared to the hyperpolarized state. This can be attributed to the absence of T-channels and low-threshold spikes (Sherman and Guillery, 2009, ch. 6) in our model. In the adapted sleep state with higher b than a, the response is shifted to an earlier phase.

Moving to the population-level response, the second row of Figure 3 superimposes the spiking networks and mean-field responses. In the awake state, the entire TC population faithfully tracks the stimulus. However, when only the TC population is set to sleep state, it responds more weakly and primarily during an initial phase, similar to the single cells response. If both populations are set to sleep mode, the TC population again responds linearly due to the adaptation a reacting slower and not as strong as spike adaptation b. Additionally, the reduced activity in the sleep state RE population leads to less inhibition and a higher amplitude of TC

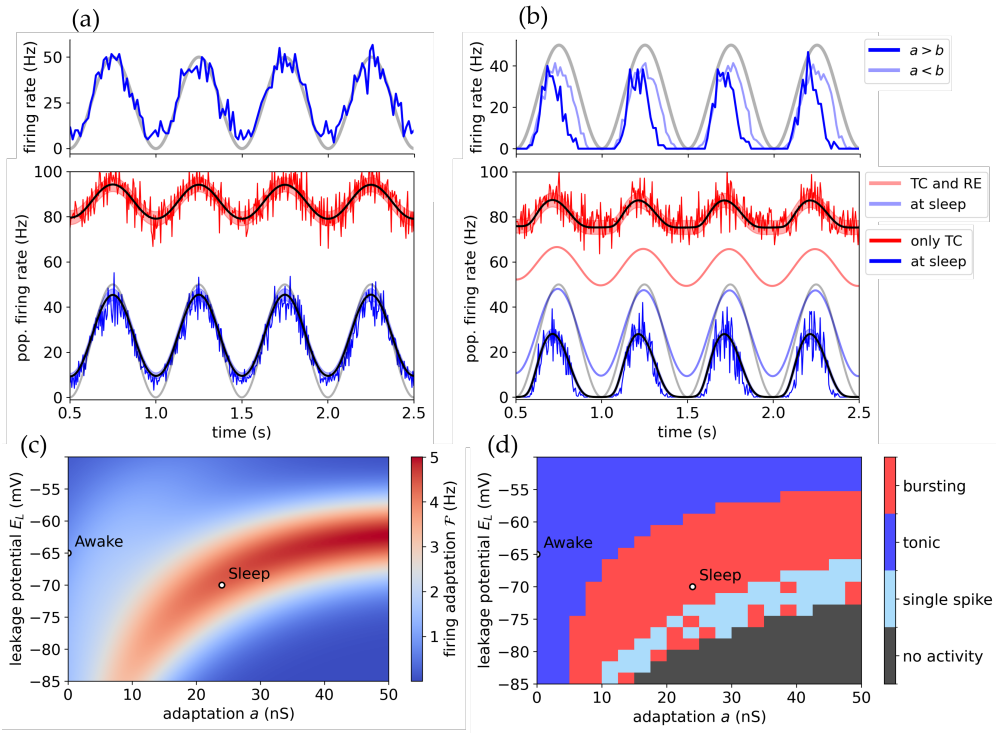

Figure 3: The impact of bursting and adaptation of TC cells in the separation of awake and sleep state. **(a)** Single cell and population response to a strong oscillatory sensory drive S in awake state. The single cell recording is taken from the same simulation as the network. In the lower plot spiking network and mean-field are superimposed. The grading stimulus is pictured in light grey. **(b)** The same setup as in (a) but in sleep and burst state (see main text). The single cell recording is done in a network which was in awake state to be close to the experiment but the population plot is done where the whole TC population (Burst) or whole network (Sleep) is in sleep mode. The single cell traces in (a) and (b) model the experiment done in Sherman and Guillery (2009, ch. 6) for tonic and bursting states of in-vivo TC recordings. **(c)** A parameter scan in both adaptation a and resting potential E_L with the mean-fields fitted transfer function (8) for TC cells, for the metric (19). Depicted are also in red the two applied states sleep and awake. **(d)** Parameter scan in a and E_L but with spiking simulations for TC cells, showing the dynamical regions of tonic, bursting and single spike states. The region of bursting between tonic and single spike firing encompasses the same subspace as the firing adaptation metric (c).

population activity so that adaptation is present at all times. Whereas if only TC are set to sleep state the time it needs the adaptation to catch up creates the shift in phase.

In conclusion, both single-cell and population-level transfer of slow, oscillatory information of TC cells appears linear in the awake (with ACh) and sleep (no ACh) states of the thalamus. However, it becomes nonlinear and phase-dependent when only TC cells are set to a sleep or hyperpolarized state, as evidenced by the single-cell traces and population responses. We made the assumption of realistic sleep-like states reducing the thalamic responsiveness (in terms of amplitude) and being more suggestive to oscillatory stimuli (as achieved by zero activity followed by a phase dependent response). This suggests that the proposition we made to define ACh depleted states as *sleep* states only holds for the case that the TC but not the RE population is set to ACh absent parameters. We will see however (in Figure 4) that this conclusion only holds for slow time-dependent inputs and with only the TC population in sleep state we need unrealistic high cortical inputs to evoke activity. Therefore, upcoming both population are set to sleep state. Furthermore, we see that a change in adaptation parameters creates the same phase-locking effect as structure depending population states at the meso-scale. These findings suggest interesting future studies for separating neuromodulator effects between relay and reticular nuclei and how different mechanisms achieve the same dynamics at different scales.

Continuing, we investigate the separation between tonic and bursting of TC cells and how this translates to the separation of defined awake and sleep states. Here we introduce a metric to quantify how adaptation shapes the response. Because the Adex generates bursting-like behaviour via its adaptation current ω, we will see a good agreement between this metric and burstiness. The approach makes use of the transfer function described in (8) and calculates a normalized difference of firing rates of a neuron type between the onset of a potential stimulus and the moment when its adaptation mechanics have reached their maximal impact and reduced the firing rate to a new equilibrium. The formalism is described in detail in the Appendix (19). By using this, we can get information about the influence of adaptation mechanisms without needing to explicitly run simulations.

In Figure 3c, we present a parameter scan calculating this metric $\mathcal{F}$ based on adaptation a and resting potential E_L parameters (using (19), including the adaptation of membrane potential). We observe distinct regions separated by high values, indicating the transition from less to strong adaptation and polarization influence. This transition is driven by a decreasing firing rate fixpoint F_ω as adaptation increases and E_L decreases. Beyond a threshold, adaptation gets to strong or the cell is too hyperpolarized and the firing rate adaptation decrease again.

To investigate in more detail our definitions of calling the ACh states bursting or tonic, we conducted a parameter scan using spiking network simulations of single TC cells based on different firing modes. Similar to (Guarino and Destexhe, 2023) and Figure 1 we injected the cell with a constant current for 1s. We classified firing patterns based on the number of spikes on a time scale relative to the adaptation time constant ($\tau_w \simeq 200$ ms). The external current applied was dependent on E_L in order to induce activity, with $I = \{200\text{nA for } E_L = -50\text{mV}, 400\text{nA for } E_L = -85\text{mV}\}$. Figure 3d presents the results, highlighting the four possible firing modes. The scan illustrates a good overlap with the adaptation metric $\mathcal{F}$, confirming the predicted similarity between firing rate adaptation and burstiness in the Adex. We see that both (c) and especially (d) agree well with our proposition of terming the ACh absent state the bursting mode of the TC cell, and that the sleep parameter state exhibits stable bursting and strong firing adaptation while the awake state is deep in the tonic regime with near to none adaptation at role.

Cortical and sensory inputs

We will proceed with how thalamic responsiveness depends on background activity.

In Figure 4a, we display the (stationary) firing rate response of the TC cell population in the mean-field model for different constant inputs via cortical and sensory drives. We applied a small constant cortical input $P = 1$Hz to be in a low activity AI state comparable to in-vivo. In case of sensory stimuli, the response is strongly proportional to the input, and we identify that the gradient of this transfer is influenced by the cortical drive P.

In Figure 4b we see this dependency is inversely proportional, where we conducted simulations for varying cortical drive strengths and observed that the response gradient decreases as P increases. This relation holds for both the awake and sleep states. Furthermore, in the sleep state, the transfer gradient remains relatively constant or even diminishes with P, contrasting the awake state's higher response gradient. This is in agreement with several studies which assumed the cortical role in the thalamus as a transfer controlling noise (see e.g. Béhuret et al., 2013).

For cortical input, the response is nonlinear but exhibits multiple linear regions, as seen in Figure 2c. The threshold between the *inhibited* and *saturated* regimes around 25Hz serves as a turning point (at which the RE population gets saturated). Inputs below this threshold do not provoke a strong response, while larger inputs do. The RE population's strong response to changes in the *inhibited* regime nearly nullifies the response.

These behaviors are evident in the TC population's response to a rectangular pulse stimulus from either P or S in Figure 4c. Notably, low cortical inputs can even be repressive, with only larger amplitudes triggering robust responses, particularly in the awake state. This is in agreement with studies such like Crandall, Cruikshank, and Connors (2015). In the sleep state or with low cortical inputs in awake state, responses are highly nonlinear, emphasizing the transfer

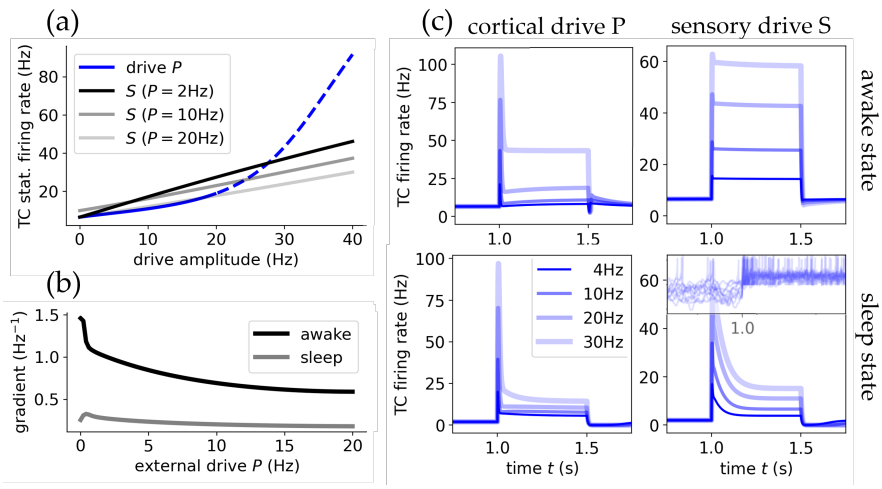

Figure 4: The thalamus' responsiveness depends on external input origin. (a) The steady state output firing rate of the TC population after reaching equilibrium for different drives P and S. Blue is for inputs coming from cortical drive P, where solid marks the *inhibited regime* and dashed the *blow-up* regime. Black are for sensory drive S, with varying degrees of cortical input. TC cells respond linearly for sensory stimuli, whereas cortical stimuli are nonlinear only showing a strong proportionality after $\sim$20Hz. **(b)** The gradients of the sensory input response curves (black in (a)) as a function of cortical input P for awake and sleep state. **(c)** The TC populations response to a rectangular stimulus of varying amplitude coming from either drive in both states. In the bottom-right there are also depicted 10 randomly chosen single cell traces to connect the population spike with single cell burst-like behaviour.

of gradients rather than absolute values. These activity spikes from gradients are created by the delay it takes the RE population to react to both stimulus and TC excitation to inhibit TC activity. This allows preserving temporal information like frequency in otherwise non-efficient response regimes and is in accordance with the occurrence of whole brain oscillatory dynamics in especially sleep-like states. Furthermore, for the awake case and sleep-like case of setting both TC and RE to no-ACh mode, no phase locking was found (compare e.g. Cakan and Obermayer, 2020 for this feature in cortical networks).

Synaptic noise

Next we move to the role of noise as background synaptic and subthreshold activity and how it influences response and firing modes. We aimed to replicate findings from (Wolfart et al., 2005). They observed that the spike and information transfer of TC neurons and the occurrence of bursts is strongly dependent on conductance noise.

We recreated this at single cell level with spiking simulations. Figure 5a shows the response of simulated single TC cells in awake state to a Poissonian spike train of 5Hz with varying excitatory synaptic strength (Q_e), reflecting the experimental setup. We observe the same step-like function in the static case without external synaptic noise: going from no activity to single spikes to bursts at high conductances (marked as dashed lines). With noise the slopes of the response function decreases and the partition of the aforementioned regimes blurres. The time-dependent noise was implemented as an Ornstein-Uhlenbeck (OU) process entering the cells membrane potential as a current (see appendix for details).

To translate this behaviour to the population level we did simulations of the full spiking network. A constant Poissonian input of 15Hz was inserted into all cells, coming from just one source; comparable to dynamical patch clamps at single cell level. The stationary output firing rate of the TC population was measured for different synaptic strengths Q_e. The resulting response function is depicted in Figure 5b for the static and noisy case for both spiking network and mean-field.

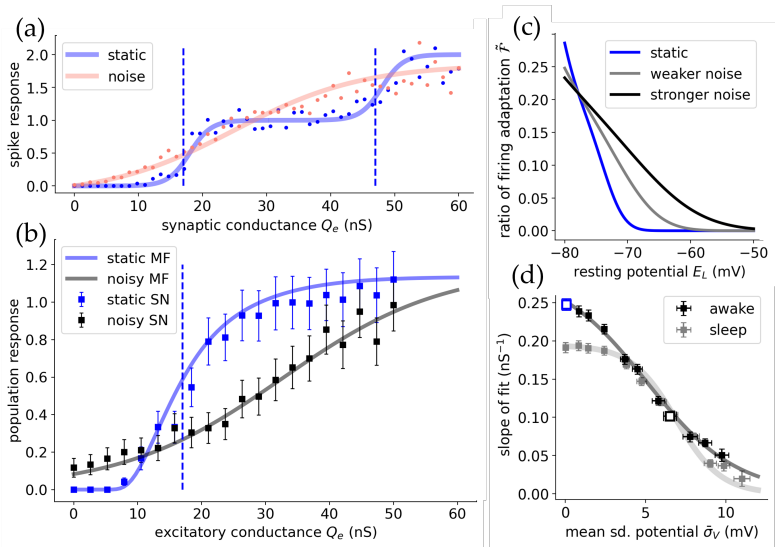

Figure 5: Noise controls responsiveness and bursting behaviour of TC cells and the thalamus. (a) Response to a 5Hz Poissonian spike train for different values of excitatory synaptic strength Q_e for simulated spiking single cells. The noise was injected as an OU-like current in the membrane potential via I_{syn}. The dots represent each the spikes per receiving incoming spike, averaged over 100 runs for 10s each. The lines correspond to sigmoidial fits, where the blue dashed lines mark the shift fit parameter depicting the center of the slope. **(b)** The same setup but with the full thalamic spiking network (squares) and the mean field (lines). The dotted line marks the slope center of the single cell simulations going from no spikes to a one-to-one spike response. For the mean-field the synaptic noise was added as a synaptic current. In there only the mean of synaptic noise is considered. To model also the standard deviation of the noise we ampted to not rewrite the mean-field formalism but to add the mean of a modeled OU-noise in each time window of size equal to the time constant of the mean-field T. (look main text) **(c)** Firing adaptation metric (as a ratio) of TC cells as a function of leakage potential E_L and for three different strength of conductance noise. Both (a) and (c) are modelled after Figure 4a and Figure 5b from (Wolfart et al., 2005). **(d)** The slopes of the mean-field transfer curves plotted against the standard deviation of the membrane potential predicted by the mean-field. Showing a proportionality between noise and slope of the transfer function and a diminishing difference between awake and sleep transfer at high noise levels.

For the mean-field, the noise-dependent transfer is passively included in the definition of the transfer function (8), with its slope being controlled by the standard deviation of the subthreshold membrane potential (σ_V). However, to recreate the experiment, which employed a time-dependent external noise, we extended the formalism by adding two additional static synaptic conductances $\tilde{\mu}_{G(e,i)}$. Those are modelled as OU-type functions averaged for each time bin T (see appendix for more details).

We see that the TC populations response function has its slope at the same place as the first step at single cell level from no activity to single spike transfer (the dashed line in Figure 5 (a) and (b), respectively). Furthermore, the role of noise is the same for population response as in the single-cell experiment, via decreasing the response functions slope.

The slope of the response function dependent on noise is depicted in Figure 5d. Here instead of the noise the noise-dependent membrane potential fluctuation averaged over all runs ($\tilde{\sigma}_V$) is shown. In sleep state the population response slope is less steep for the static case or small noise. Strong noise and subsequent membrane potential fluctuations decrease the slope as expected and also equalize the response function between awake and sleep state at higher noise levels, in an equal manner as in the single cell experiment (Wolfart et al., 2005).

Finally, we produce another experiment done in Wolfart et al. (2005). In Figure 5c it is shown that the firing rate adaptation ($\mathcal{F}$ via (19)) depends on the polarisation of the cell, but that noise here also acts as an equalizer and increases the firing adaptation capability of cells at also resting and depolarised membrane potential values. This is in agreement with how

experimentally fluctuations act on TC cell's burstiness and further supports the similarities between $\mathcal{F}$ and bursting capabilities.

Spindle oscillations

Spindle oscillations are one of the main activity dynamics of the thalamus during slow-wave sleep or anesthesia (Steriade, 2003), strongly influencing the responsiveness of the thalamus in such states. These originate from the superposition of multiple cellular and circuit properties. In ACh depleted conditions such as during sleep, T-channel currents promote bursts after hyperpolarization (as modeled in Destexhe, Contreras, and Sejnowski, 1994 for a Hodking-Huxley model), and barrages of IPSPs occur in strongly connected subgroups within the TRN (Shu and McCormick, 2002). This creates two self-sustained loops: an inhibitory self-loop within TRN neurons, and a loop connecting RE and TC cells (see colored connections in Figure 6e). The rebound bursts caused by this circuit arrangement generate spindle oscillations, as shown by experiments and computational models (Destexhe and Sejnowski, 2001; Steriade, 2003).

Computational models demonstrated that a 4-neuron structure of TC and RE neurons exhibits self-sustained oscillations with all characteristics of spindles, as shown first for Hodgkin-Huxley type models (Destexhe, Bal, et al., 1996) and later using AdEx models (Destexhe, 2009). These oscillations rely on a loop where a TC cell triggers a burst in an RE cell, which, in turn, causes a rebound burst in another TC cell, completing the cycle. In their study, however, the oscillations waned with increased network size.

In this study, we want to show that the proposed models in a sleep-like state indeed show spindles at all scales, validating them as thalamic models. In contrast to Destexhe (2009), we aim for robust spindles at population scales. To enhance rebound bursting we promote burst firing by adjusting the reset membrane potential (V_r) below the sodium spike threshold onset: $V_r = -48$mV for TC and $V_r = -42$mV for RE cell. This yields sustained burst firing without sustained activation, mimicking T-channel like activation and IPSP barrages in RE cells. Accordingly we re-calibrate the mean-field fit to accommodate the change in V_r. (The original fit produces spindles too, but with unrealistic amplitudes.) The resulting fit parameters are depicted in Table 3.

In Figure 6b we illustrate oscillatory dynamics in a small network of 20 neurons, revealing a generating 4-loop structure inside the network (a). We employed the burst-adjusted sleep parameters but with synaptic parameters from Destexhe (2009). To invoke activity, an initial kick of Poissonian input of high frequency to only a random subset of neurons was applied.

Moving to the network size of $N = 1000$ neurons used in this study, we employ our full parameter set (Table 1) and the same kick. We show in Figure 6c that the full spiking network shows self sustained oscillations.

For the mean-field to produce self-sustained oscillations we employ the 4-structure as seen at single cell level (from Destexhe, 2009) and justify its need also at the population level. This is further supported by studies such as McCormick, McGinley, and Salkoff (2015). They showed the mechanism behind the generation and specific frequency of oscillations in the thalamus is the delay in the propagation of activity between different TC neurons. Thalamic relay cell clusters have no connection to themselves and so RE neurons serve as intermitter. The slow adaptation mechanics governing rebound bursts are therefore generating the slow ~ 10Hz spindle oscillations.

In order to implement this, we construct two RE and two TC populations and keep all connections active, but reduce the connection probability of links which are antagonistic to this propagation via rebound bursts. This can be seen as two close but locally separated subgroups of relay neurons. The resulting structure is depicted in Figure 6e. (Note: If the connections are set homogeneous then this network is acting exactly like a mean-field with just two populations.) The main links for the propagation are colored and labeled with their mechanism of propagation: RE induced rebound bursts and TC excitation. To initiate the spindles here also a kick of high activity going to only one or two populations was necessary, in agreement with the spiking network. Additionally, T was set to 15ms to have similar phases and shapes with the spiking network. The averaged spiking network and resulting mean-field

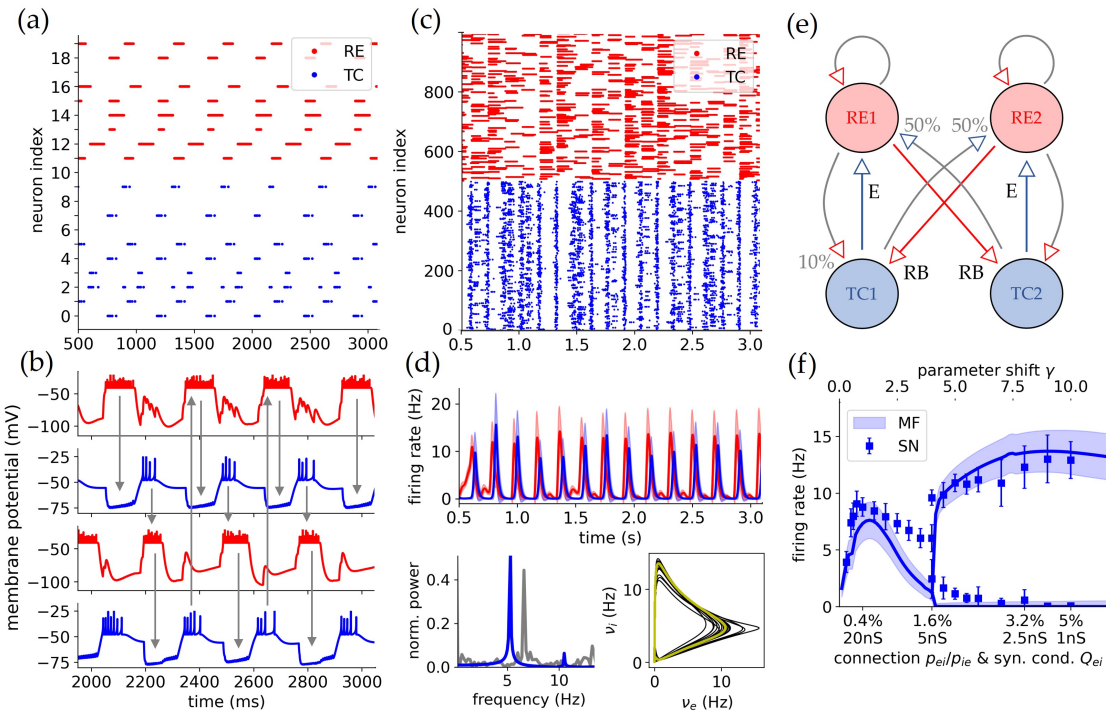

Figure 6: Spindle-like oscillations are generated by the special TC-RE connections and missing excitatory-excitatory links in the thalamus. (a) Raster plot of the simulation for the small network showing all 20 neurons. **(b)** Four neurons showing anti-phase burst firing with rebound bursts of the TC cells as a possible generator of spindles. Cell traces are taken from the simulation in (b) with a small network ($N = 20$). The arrows show the loop of activity propagation between RE and TC cells with rebound bursts and direct excitation. These pathways translate to the four colored ones in (e) at population level. **(c)** Raster plot of the full-scale spiking network with 1000 neurons for spindle parameters (ACh/sleep state with rebound burst). **(d)** Mean-field oscillations. Top: firing rates and standard deviations. Bottom left: Fourier spectrum for spiking network (grey) and mean field (blue) of the TC population activity. Bottom right: Phase plane in the TC and RE firing rate space. Red is the stable limit cycle. **(e)** The 4-structure used for the mean-field connections. The colored arrows mark the main pathway of propagation with rebound bursts (RB) and excitation (E) as transmitters. The non-significant connections are marked in grey with their respective relative strength shown in percentages of the original connection probability. The RE populations keep their local self-loop. **(g)** Bifurcation diagram showing the suggested Andronov-Hopf bifurcation that occurs when gradually increasing the connection probability in the network, for spiking network and mean-field. This corresponds to a parameter shift from the parameters used in Destexhe (2009) with $\gamma = 1$ to the parameters used in this paper with $\gamma = 10$.

activities of the populations are depicted in Figure 6c. In the bottom row we compare the Fourier spectrum and show the transient into the stable limit cycle.

In contrast to these oscillations occuring at larger ($N = 1000$) scales, in Destexhe (2009) small networks generated spindles in SR-like dynamics while at scales of $N > 40$ neurons population activity produced self-driven steady states with AI dynamics. In Figure 6g we show a bifurcation diagram transitioning between connection and balancing synaptic parameters from Destexhe (2009) ($\gamma = 1$) to our parameter values (Table 1, $\gamma = 10$). Showing that sufficient connections are necessary for spindles at larger scales. The Jacobian eigenvalues calculated at the steady points of the mean-field up to the bifurcation point are complex. This together with the transition into a stable limit cycle suggests a supercritical Andronov-Hopf bifurcation as the origin of spindles.

This self-sustained oscillation is remarkably robust in regards to perturbations of all kinds of inputs, with even oscillatory inputs producing the same frequency spindles. This renders the thalamus' responsiveness in this spindle-adjusted sleep state relatively independent of external

input. Only prolonged and constant inputs of a duration longer than multiple spindle periods destroy the synchronisation and create steady state AI dynamics, with the spindles however starting again after the input stops. Furthermore, the bifurcation diagram in connection with Destexhe (2009), shows that thalamic function and responsiveness can be drastically altered depending on specific order parameters, such as here with network and synaptic parameters.

DISCUSSION

In this study, we investigated the state-dependent responsiveness of the thalamus at micro to meso scale. For this we introduced a biologically realistic spiking and mean-field model of the thalamus, which capture the population dynamics of thalamo-cortical relay neurons (TC) and thalamic reticular neurons (RE) in both awake and sleep-like states.

The mean-field model employs the master-equation formalism introduced by El Boustani and Destexhe (2009) and incorporates adaptation mechanics (DiVolo et al., 2019). We constructed it using a bottom-up approach following the formalism described by Zerlaut et al. (2016), which includes a subthreshold-dependent transfer function. This unique feature allows us to connect firing rates with membrane potential dynamics and realistic cell parameters in a meaningful way. With this it is possible to construct a cell-specific transfer function based on the Adex model from either single cell simulations or electrophysiology. We built a thalamic network structure faithful to experimental observations, showing that both the mean-field and spiking network exhibit the wanted balanced excitation-inhibition state with AI dynamics, and with a dominant and controlling RE activity.

We successfully validated the mean-field's predictive accuracy through comparison with the spiking network, confirming its ability to replicate the dynamic behavior and population distribution of thalamic cells. We also demonstrated that the mean-field model is capable of predicting the network's subthreshold activity and proved its validity beyond the fitting point. This allowed us to explore the global parameter space and apply methods to simulate experiments. For example this allows the use of experiments using intracellularly injected currents in combination with this model.

The focus of this study on responsiveness of the thalamus and how it depends on internal and external state, was investigated in three steps:

First, we revealed the role of bursting in TC cells as a linear-nonlinear switch in the transfer of sensory stimuli at a macro scale, in agreement with the findings of Sherman and Guillery (2009). This transition between tonic and bursting firing patterns in TC cells provides a mechanism by which the thalamus modulates the transmission of sensory information to the cortex. However, we found that in the proposed sleep state, the transfer of slow oscillatory stimuli remains linear, as in the awake case, but becomes nonlinear and phase-dependent only if the TC cells, not the RE cells, exhibit sleep-like ACh neuromodulation. This is due to the RE population also experiencing reduced activity in its hyperpolarized sleep state. This finding underscores the importance of incorporating biological single-cell parameters and dynamics into population-level models but to also include real structure. We also showed the use of the mean-field formalism for analytical approaches and found a metric counting the change of firing rate to adaptation, comparable to burstiness measures with the Adex, resulting in an efficient method for parameter scans.

Second, we examined the influence of external states on thalamic response. We demonstrated that in this model, there is an important distinction in the origin of inputs: sensory-like stimuli experience a more linear response and are therefore transferred more faithfully than cortical-like inputs, which generate a nonlinear response. We also identified the capability of cortical inputs, passing through TRN neurons and activating them, to significantly increase inhibition in the thalamus, thereby repressing response and transfer of stimuli. However, in the sleep state, we showed that the relay of information becomes strongly nonlinear regardless of input origin. Because of the cells' bursting capabilities and delayed inhibitory feedback from RE neurons, phase and frequency of strong gradients are still transferred. This aligns with findings about whole brain oscillations and their propagation during sleep-like states.

Third, we investigated the role of synaptic noise in thalamic response. The experimental findings of Wolfart et al. (2005) were as a first time successfully modeled. We demonstrated that synaptic noise acts as a controller for response also at the population level. The TC cells' step-like transfer function in response to single spikes translates well into their collective response at population scale, both response functions sharing the same conductance threshold for activity. This allows the thalamus to fine-tune its responsiveness to external stimuli. However, the transition from single to double spike response at high conductances does not influence the populations response. Furthermore, noise acts as an equalizer between states of awake/sleep at the population level and tonic/bursting firing at the cell level. This insight contributes to our understanding of the thalamus's adaptive capabilities, particularly in the context of sensory processing. And that more hidden elements such as subthreshold noise–which are often not included in modelling approaches–can show great impact at even macro scales.

Finally, the successful reproduction of spindle-like oscillations in a sleep-like state is an important validation for our thalamic model. We emphasize the necessity of specific substructures within the thalamus for generating oscillations at all scales. Additionally, with this structural explanation of spindles, and in agreement with experiments (Brunel and Hakim, 2008), the neurons keep their AI dynamics during such oscillations. In this state thalamic responsiveness to inputs is highly suppressed, keeping stable spindle oscillations. Only strong and prolonged inputs temporarily create AI dynamics while they are active. This investigation showed that order parameters, such as in this case connection probability and synaptic conductance, can have a great impact on responsiveness via introducing new phase transitions and population dynamics.

Here however, the spindle-adjusted sleep state differs quite substantially from the sleep state in the rest of this study. The adapted leakage and reset parameters, modelling T-channel like activation and IPSP barrages to invoke stronger rebound bursts, create this significant difference, suggesting two distinct states. One representing a sleep state similar to N2 in which spindles are observed, while the other could represent a less-deep sleep state. This suggests that the concentration of ACh alone is not sufficient for investigating awake and sleep separation, but the mechanisms behind rebound bursts are specifically important to include. Especially how these connect to ACh and other, in this study neglected, neuromodulators like dopamine, norepinephrine, or serotonin. Additionally, we remark that the shown spindles inherit the correct underlying mechanisms, as evident from experiments, but do show a frequency at the lower end of the usually defined spindle frequency, potentially being more close to Delta waves. All this hints at interesting future work in connecting physiological brain states of awake and sleep with multi-scale thalamic models.

In conclusion, our study underscores the value of integrating single-cell dynamics with thalamic specific structure at population-level in understanding the complex role of thalamic responsiveness and accordingly for sensory processing and cognitive functions. This study advances our comprehension of thalamic function through its modeling of bursting, noise and cortical feedback, and how these states change thalamic function and response. Additionally, in combination with experimental papers we support a very specific way of how spindle oscillations are generated in the thalamus and influence its response in a deep sleep-like state. With these findings and with offering a biologically realistic and experimentally grounded meso-scale model of the thalamus, we provide here an essential starting point for further investigation of thalamic function and physiological states connected to micro scale effects such as neuromodulators. In connection with previously developed cortical mean-field models, this also serves as crucial step towards large-scale thalamo-cortical simulations of multiple brain areas. These would allow to bridge the gap between cell and synaptic behaviours with studies incorporating overall brain pathways, including behavioral neuroscience, neural disorders, and prosthetics.

APPENDIX

Additional formulae

The double Gaussian stimulus used as an input is defined as

$$G(t, t_0) = A\big(\theta(t_0 - t)\mathrm{e}^{\frac{-(t-t_0)^2}{2\sigma_l^2}} + \theta(t - t_0)\mathrm{e}^{\frac{-(t-t_0)^2}{2\sigma_r^2}}\big), \tag{15}$$

with amplitude θ and slopes $\sigma_{l,r}$ of the left and right half-side Gaussian, respectively.

Ornstein-Uhlenbeck type noise can be defined as

$$\frac{\mathrm{d}x}{\mathrm{d}t} = \theta(\mu - x) + \sigma\frac{\mathrm{d}W}{\mathrm{d}t}, \tag{16}$$

where μ is the mean reversion level, θ the mean reversion rate, and σ the amplitude of the standard Wiener process $W(t)$, or white noise.

The conductance noise was implemented in the mean-field via adding the mean of OU-type noise (x) in a time window corresponding to T to the static conductances μ_G (see methods). The resulting conductances including noise are then:

$$\tilde{\mu}_{G(e,i)} = \mu_{G(e,i)} + \overline{x(t)^T_{(e,i)}}. \tag{17}$$

The specific parameters for x used for the synaptic noisy case in most simulations are $\mu = 0\text{nS}$, $\theta = 5\text{ms}^{-1}$, and especially $\sigma_i = 200\text{nS}$ and $\sigma_e = 60\text{nS}$ for the amplitudes.

The differential equation describing the correlation of populations $\{\mu, \nu, \lambda\} \in \{e, i\}$ to close the second order statistical moments of the mean-field formalism is given by

$$T\partial_\tau C_{\mu\nu}(\tau) = (\partial_\lambda F_\nu \cdot \nu^0 - \delta_{\lambda\nu})C_{\mu\lambda}(\tau), \tag{18}$$

where τ is the time lag and ν^0 marks the stationary solution of the firing rate.

Dynamical analysis

The steady and equilibrium points of the spiking network are taken as the averaged population activity over long simulation times for constant inputs where oscillations are ruled out either by observation or by spectrum analysis. For the mean-field these are calculated as the populations activity after a transient up to a point where the Jacobian (J) eigenvalues are negative. The Jacobian is defined on the variable set $X \in \{\nu_e, \nu_i, \omega_e, \omega_i\}$ and calculated via numerical derivatives.

For the bifurcation diagram (Figure 6) the same technique was used up to the bifurcation point, except that now $X \in \{\nu_e^1, \nu_e^2, \nu_i^1, \nu_i^2, \omega_e^1, \omega_e^2, \omega_i^1, \omega_i^2\}$. For the mean-field the Jacobian eigenvalues are complex up to the bifurcation point, suggesting a supercritical Andronov-Hopf bifurcation. After the bifurcation point for the spiking network, instead of the averaged firing rates, the extrema are averaged over a long time simulation, mimicking the real sub-plane of the complex space Andronov-Hopf bifurcation. The same was done for the mean-field.

The maximum Lyapunov exponents are calculated numerically employing the Rosenstein algorithm (Rosenstein, Collins, and De Luca, 1993).

Numerical simulations

All simulations were conducted in `Python`. The spiking network simulations additionally used the `Python` package `Brian2` (Stimberg, Brette, and Goodman, 2019). Constructing the network, all neuron connections to random to ensure a statistical model comparable to the mean-fields assumptions. All numerical integrations in spiking network simulations employed *Heun's method*, while for mean-field simulations *Euler's method* was used.

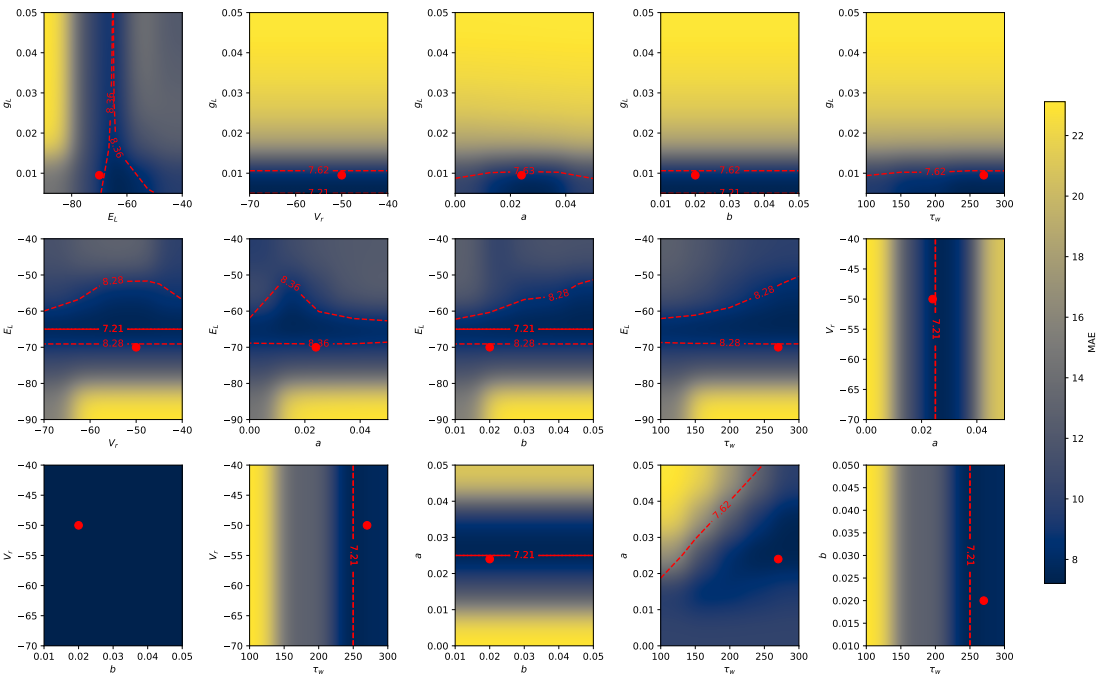

Figure 7: Parameter space fit for TC without ACh. The *mean absolute error* (MAE) between the Adex (1) and the TC cell traces in absence of ACh from McCormick and Prince, 1986. Red lines mark minimum MAE (solid lines) and 5% deviation from said minimum (dashed lines). The employed parameter values are marked as the red dot. (see units in Figure 9)

Firing adaptation metric

The approach makes use of the transfer function F described in (8). For the effect of adaptation mechanics on the firing rate of a neuron type we can identify two crucial states: The no-adaptation fixpoint (F_0): This state represents the firing rate of a cell in the absence of adaptation and corresponds to the cell's firing rate at the onset of a stimulus where the (slow) adaptation mechanics have no impact yet. And the real-adaptation fixpoint (F_ω): Representing the cell's firing rate when it has fully adapted to its own and the stimulus influence. Then $F_0 - F_\omega$ reflects the change in firing rate of a cell from initial activity at the onset of a stimulus as it transitions towards full adaptation and slowing its firing rate.

Necessarily, the transfer function is firing-based and needs non-zero firing rate inputs (ν_e, ν_i) to yield results. Therefore, we calculate the fixpoints for a constant $\nu_e = 1\text{Hz}$. By normalizing and multiplying with F_ω we quantify the metric in not only the saturation of firing rate but also the actual firing rate during the stimulus. This yields a ratio between the highest firing rate and the fully adapted one. When considering high firing rates as decreased ISIs this metric is comparable to experimental methods measuring burstiness (such as Wolfart et al., 2005). Concluding, we define this metric as

$$\mathcal{F} \equiv \frac{F_0 - F_\omega}{F_0} \cdot F_\omega, \quad \text{where} \quad \partial_t F_x(\nu_e = 1\text{Hz}, \omega = x) = 0 \quad \text{with} \quad x \in \{0, \omega\}. \tag{19}$$

Additionally, we can include the differences in membrane potential between high and low firing states into the calculation (This provided better agreement with the spiking simulation in Figure 3c). We incorporate the membrane potential by multiplying (19) with a similar fixpoint term $(\mu_V^0 - \mu_V^\omega)/\mu_V^0$.

SUPPLEMENTARY MATERIAL

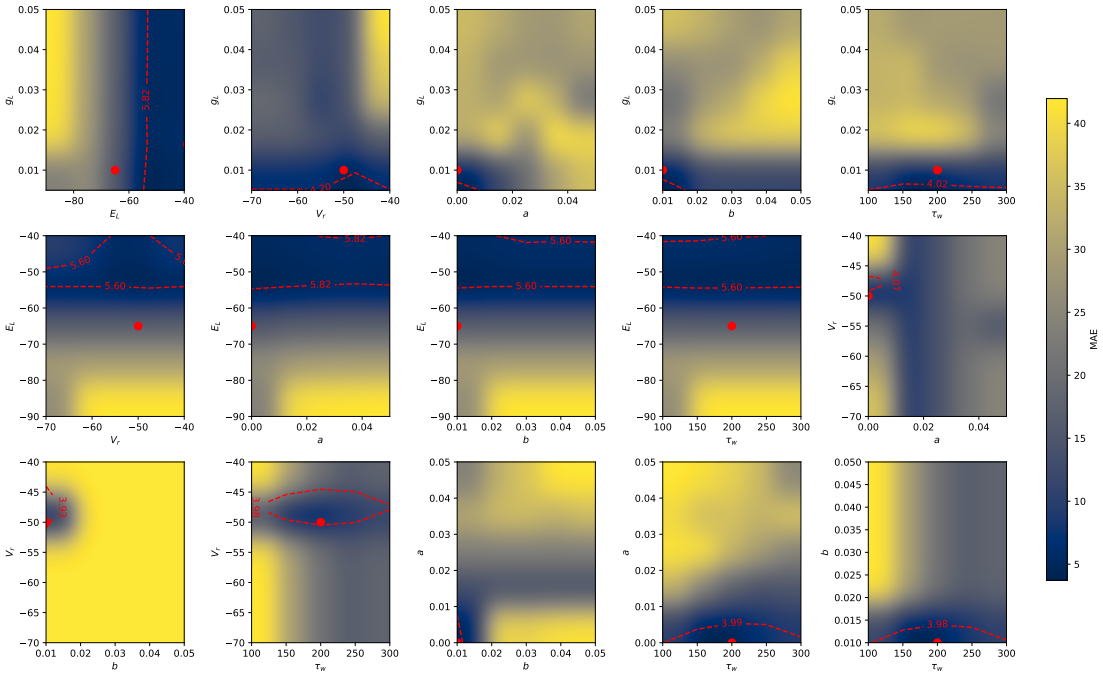

Figure 8: Parameter space fit for TC with ACh. (see caption in Figure 7 and units in Figure 9)

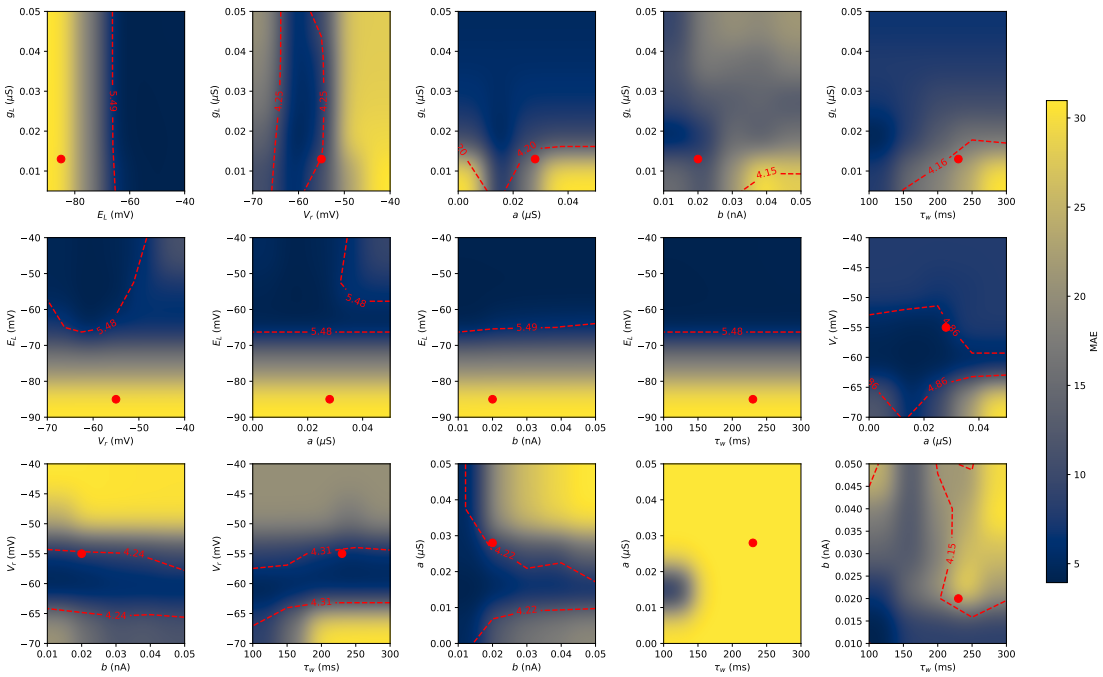

Figure 9: Parameter space fit for RE without ACh. (see caption in Figure 7) The chosen value of E_L marks the biggest MAE. Here we still chose to take a hyperpolarised value to account for the reduced excitability in RE neurons with ACh absent (McCormick and Prince, 1986) and to inhibit also the population response to keep the stability of the network. (see main text)

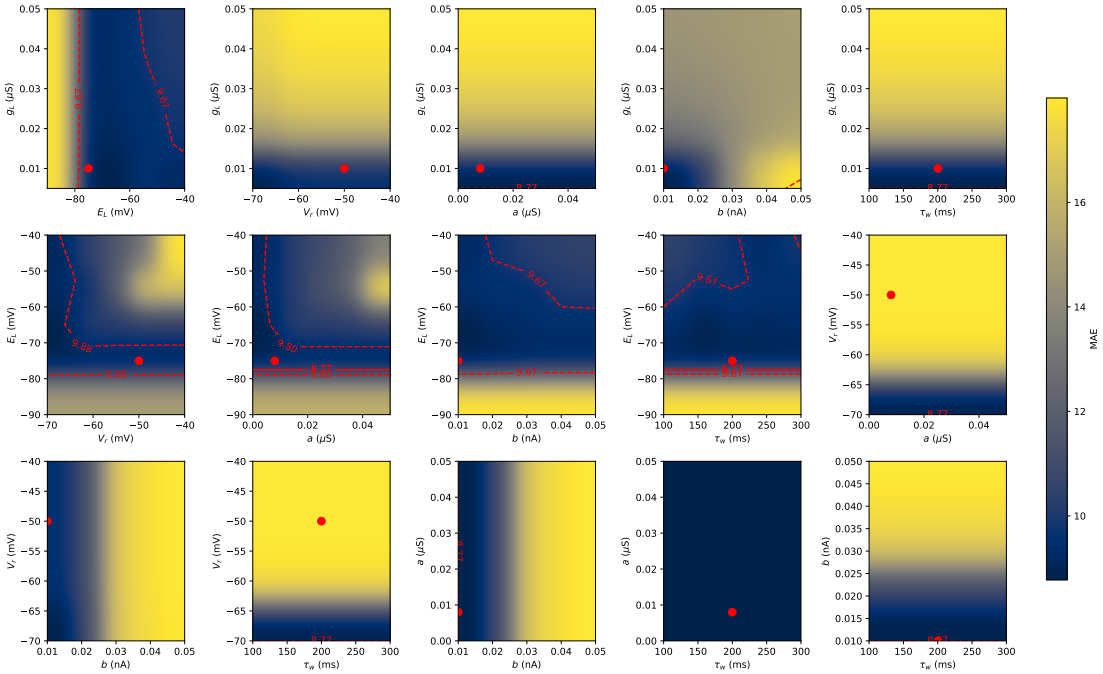

Figure 10: Parameter space fit for RE with ACh. (see caption in Figure 7)

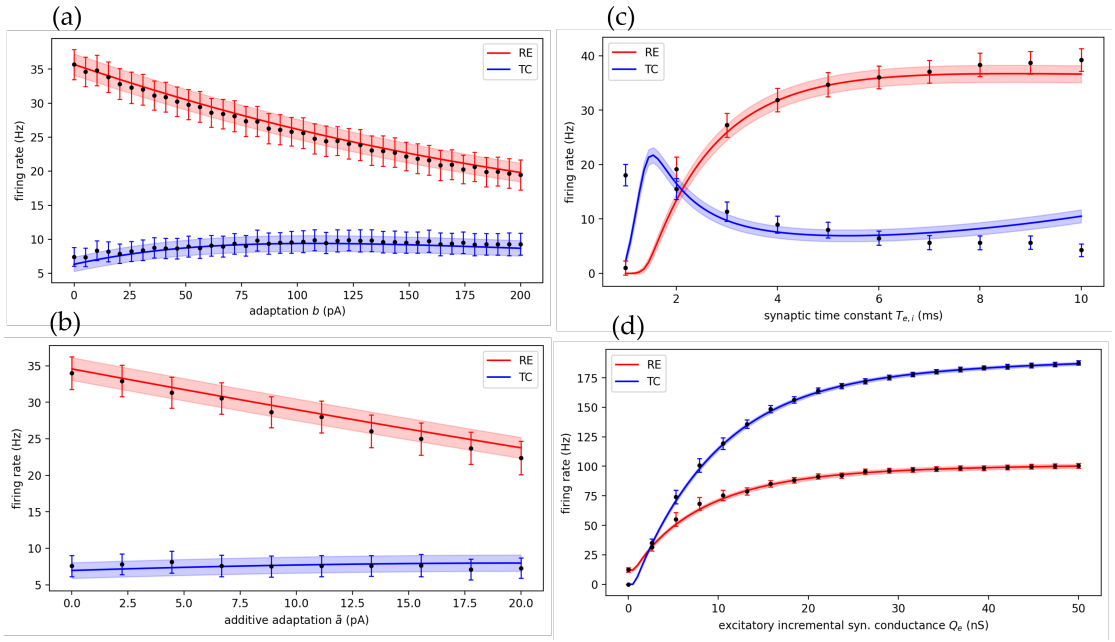

Figure 11: Global parameter analysis between mean-field and spiking network. Markers represent equilibrium population firing rates of the spiking network. Line and shaded area represent the mean-fields mean and standard deviation, respectively. **(a)** Spiking adaptation parameter. **(b)** Membrane potential adaptation parameter as shift on the original ones to keep the difference between TC and RE adaptations securing stable dynamics. (a) and (b) ensure the mean-fields validity between awake and sleep state. **(c)** Synaptic exponential delay time constant of both populations. **(d)** Excitatory incremental synaptic conductance for TC only. This allows modeling dynamic clamp-like techniques and changing or *injecting* conductances.

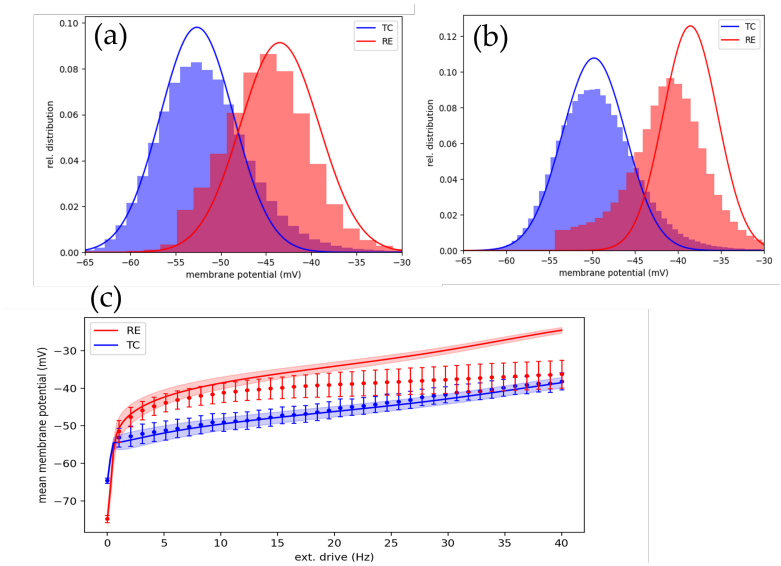

Figure 12: The mean-fields prediction for membrane potential dynamics in comparison to spiking networks is quite accurate but falls off at high firing rate states. One shortcoming of the formalism is that it only considers the linear part of the Adex equation (1). This leads at higher (input) firing rates to a missmatch because there each neuron experiences a significant depolarisation and is staying more in the onset region of the spike. This region experiences a great impact by the exponential term in the Adex which in term increases ν so that this region leads directly to spikes. Therefore, the nonlinear influence grows with increasing excitation of the cell and produces a left shift of the network distribution. This can be seen in (b) which was recorded at a higher firing rate than (a). The second deviation of the formalism compared to the spiking model is that the spike detection and reset mechanism forces two constant hard cuts into the simulation. These restrict the membrane potential with an upper limit but also–and more significantly–let all cells reset to the same value for a refractory period after a spike. This is accounted for in all figures: where the cells membrane potential ν has the exact value as the reset value V_r these points are removed from the distribution. The deviation grows with increased drive. Shown in (c) is a comparison for equilibrium mean μ_V and standard deviation σ_V between spiking network and mean-field. We can see that the above described shortcoming of the linear formalism explains the discrepancy in the RE membrane potentials at higher frequency.

Table 3: The fitting parameter values for recreating spindles with sleep parameters and included rebound burst mechanics. All values in mV.

cell	P_0	P_μ	P_σ	P_τ	$P_{\mu\mu}$	$P_{\mu\sigma}$	$P_{\mu\tau}$	$P_{\sigma\sigma}$	$P_{\sigma\tau}$	$P_{\tau\tau}$
TC	−51.17	3.94	15.53	−7.15	0.35	−7.57	−1.19	−13.61	9.47	29.44
RE	−45.84	3.53	−16.90	41.75	0.34	2.02	−5.23	19.44	49.70	−93.53

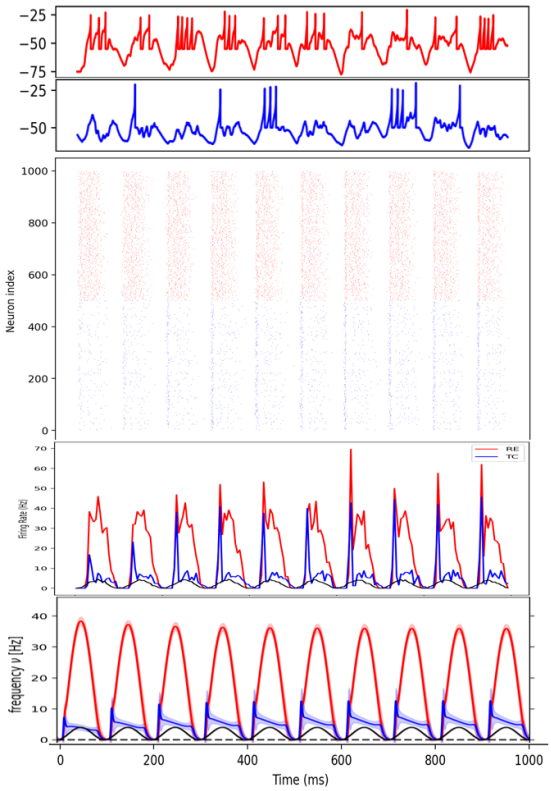

Figure 13: Activity bursting leads to transfer in a strongly inhibitory controlled thalamus. We applied a cortical oscillatory drive P with an amplitude of 4Hz and a frequency of 10Hz. Going from top to bottom, first there are depicted two randomly chosen single cell traces of RE and TC and the whole raster plot of the two populations. The raster plot shows all spiking times $\{t_s\}$ of each neuron. The population spikes follow the oscillatory drive and in the single cell plots the neurons show *bursting like* behaviour, especially at the onset of the stimulus. Based on the single cell dynamics we can state that the observable bursting like activities in RE cells correspond to real bursting, whereas the TC cell shows only high firing rate states but no biological bursting. In Figure 2[c] one can see that the respond of the TC population–as a function of cortical drive P–increases to a plateau level and stays there until the RE population activity saturates. This plateau leads to the TC population responding only minimal to a change in cortical stimulus. The reason for this is the strong inhibition inherent in the thalamus and also in our model. This plateau should mean that time dependent inputs like oscillations will not be transferred in a linear fashion. Whereas the RE activity should react to P more or less linearly. We can see exactly that in the population activities from network and mean-field in response to the oscillatory drive P in the bottom two plots, showing network and mean-field activities. The RE firing rate follows the oscillation nicely, whereas the TC firing rate is saturating and not following the stimulus linearly. However, we can see a spike or burst in activity at the onset of each period of the stimulus. There the system is in a state in the early region of Figure 2[c] where the TC response is strong first and with increasing drive the RE population gets activated and in term inhibits and enforces the plateau on the TC activity. This transient region preceding the plateau, therefore, allows the TC to respond to a changing stimulus strongly before the RE population gets activated by either an increasing drive or by the TC cells themselves, and inhibiting the TC cells. This mechanism leads to *activity bursting*. This behaviour is determined by the fast responding TC cells and the strong inhibitory nature of the RE cells of the thalamus, and allows a transfer of information via these bursts coming from the cortex, even though the cortex strongly acts on the inhibiting RE cells.

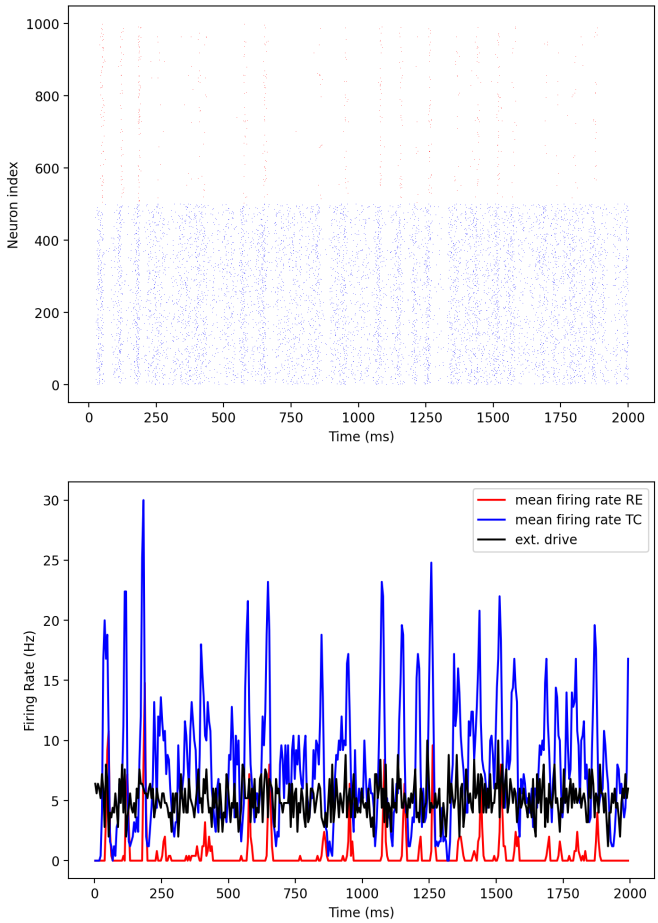

Figure 14: We observed that if the ratio $S/P \gg 1$ for small P then the spiking network starts to oscillate at γ frequencies. This behaviour will not be further investigated here but is the reason behind a non-zero *background* drive P in all simulations if there is an active non-negligible drive S.

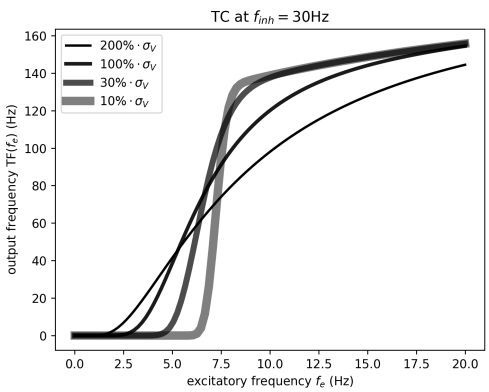

Figure 15: The slope of the transfer function F is governed by the membrane potentials *noise* (σ_V).

AVAILABILITY

All code will be handed out tailored to specific requests. The numerical codes for simulating mean-field and spiking network are also freely available at the corresponding `GitHub` page: https://github.com/SiodhachanOSullivan/Thalamic-mean-field.

AUTHOR DECLARATIONS

The authors declare no competing conflict of interests.

ACKNOWLEDGMENTS

Research supported by the CNRS and European Union (Human Brain Project H2020-945539, and ERASMUS+ scholarship).

REFERENCES

Amit, Daniel J., Hanoch Gutfreund, and H. Sompolinsky (Aug. 1985). "Spin-glass models of neural networks". In: *Phys. Rev. A* 32 (2), pp. 1007–1018. DOI: 10.1103/PhysRevA.32.1007. URL: https://link.aps.org/doi/10.1103/PhysRevA.32.1007.

Bassett, Danielle S., Perry Zurn, and Joshua I. Gold (2018). "On the nature and use of models in network neuroscience". In: *Nature Reviews Neuroscience* 19, pp. 566–578. URL: https://api.semanticscholar.org/CorpusID:205569660.

Béhuret, Sébastien et al. (Dec. 2013). "Cortically-Controlled Population Stochastic Facilitation as a Plausible Substrate for Guiding Sensory Transfer across the Thalamic Gateway". In: *PLoS computational biology* 9, e1003401. DOI: 10.1371/journal.pcbi.1003401.

Bellay, Timothy et al. (July 2015). "Irregular spiking of pyramidal neurons organizes as scale-invariant neuronal avalanches in the awake state". In: *eLife* 4. Ed. by Frances K Skinner, e07224. ISSN: 2050-084X. DOI: 10.7554/eLife.07224. URL: https://doi.org/10.7554/eLife.07224.

Breakspear, Michael (2017). "Dynamic models of large-scale brain activity". In: *Nature Neuroscience* 20, pp. 340–352. URL: https://api.semanticscholar.org/CorpusID:20538785.

Brette, Romain and Wulfram Gerstner (Dec. 2005). "Adaptive Exponential Integrate-And-Fire Model As An Effective Description Of Neuronal Activity". In: *Journal of neurophysiology* 94, pp. 3637–42. DOI: 10.1152/jn.00686.2005.

Brown, RE et al. (2012). "Control of sleep and wakefulness." In: *Physiol Rev.* 92.3, pp. 1087–187. DOI: 10.1152/physrev.00032.2011.

Brunel, Nicolas and Vincent Hakim (Mar. 2008). "Sparsely synchronized neuronal oscillations". In: *Chaos: An Interdisciplinary Journal of Nonlinear Science* 18.1, p. 015113. ISSN: 1054-1500. DOI: 10.1063/1.2779858. eprint: https://pubs.aip.org/aip/cha/article-pdf/doi/10.1063/1.2779858/14599104/015113_1_online.pdf. URL: https://doi.org/10.1063/1.2779858.

Cakan, Caglar and Klaus Obermayer (Apr. 2020). "Biophysically grounded mean-field models of neural populations under electrical stimulation". In: *PLOS Computational Biology* 16, e1007822. DOI: 10.1371/journal.pcbi.1007822.

Castro-Alamancos, Manuel A. and Barry W. Connors (1996). "Cellular Mechanisms of the Augmenting Response: Short-Term Plasticity in a Thalamocortical Pathway". In: *Journal of Neuroscience* 16.23, pp. 7742–7756. ISSN: 0270-6474. DOI: 10.1523/JNEUROSCI.16-23-07742.1996. eprint: https://www.jneurosci.org/content/16/23/7742.full.pdf. URL: https://www.jneurosci.org/content/16/23/7742.

Coombes, Stephen (Sept. 2005). "Coombes, S.: Waves, bumps, and patterns in neural field theories. Biol. Cybern. 93(2), 91-108". In: *Biological cybernetics* 93, pp. 91–108. DOI: 10.1007/s00422-005-0574-y.

Crandall, Shane R., Scott J. Cruikshank, and Barry W. Connors (2015). "A Corticothalamic Switch: Controlling the Thalamus with Dynamic Synapses". In: *Neuron* 86.3, pp. 768–782. ISSN: 0896-6273. DOI: https://doi.org/10.1016/j.neuron.2015.03.040. URL: https://www.sciencedirect.com/science/article/pii/S0896627315002640.

Destexhe, Alain (July 2009). "Self-sustained asynchronous irregular states and Up–Down states in thalamic, cortical and thalamocortical networks of nonlinear integrate-and-fire neurons". In: *Journal of computational neuroscience* 27, pp. 493–506. DOI: 10.1007/s10827-009-0164-4.

Destexhe, Alain, Thierry Bal, et al. (1996). "Ionic mechanisms underlying synchronized oscillations and propagating waves in a model of ferret thalamic slices." In: *Journal of Neurophysiology* 76, pp. 2049–2070.

Destexhe, Alain, Diego Contreras, and Terrence Sejnowski (Aug. 1994). "A Model of Spindle Rhythmicity in the Isolated Thalamic Reticular Nucleus". In: *J Neurophysiol* 72.

Destexhe, Alain and Terrence J. Sejnowski (2001). *Thalamocortical Assemblies.* Oxford University Press, Oxford UK. ISBN: 0-19-852425-0.

DiVolo, Matteo et al. (Apr. 2019). "Biologically Realistic Mean-Field Models of Conductance-Based Networks of Spiking Neurons with Adaptation". In: *Neural Computation* 31.4, pp. 653–680. ISSN: 0899-7667. DOI: 10.1162/neco_a_01173. eprint: https://direct.mit.edu/neco/article-pdf/31/4/653/1050655/neco_a_01173.pdf. URL: https://doi.org/10.1162/neco%5C_a%5C_01173.

Doron, Guy et al. (2014). "Spiking Irregularity and Frequency Modulate the Behavioral Report of Single-Neuron Stimulation". In: *Neuron* 81.3, pp. 653–663. ISSN: 0896-6273. DOI: https://doi.org/10.1016/j.neuron.2013.11.032. URL: https://www.sciencedirect.com/science/article/pii/S089662731301129X.

El Boustani, Sami and Alain Destexhe (Jan. 2009). "A Master Equation Formalism for Macroscopic Modeling of Asynchronous Irregular Activity States". In: *Neural Computation* 21.1, pp. 46–100. ISSN: 0899-7667. DOI: 10.1162/neco.2009.02-08-710. eprint: https://direct.mit.edu/neco/article-pdf/21/1/46/818085/neco.2009.02-08-710.pdf. URL: https://doi.org/10.1162/neco.2009.02-08-710.

Gent, TC et al. (2018). "Thalamic dual control of sleep and wakefulness." In: *Nat Neurosci.* 21.7, pp. 974–984. DOI: 10.1038/s41593-018-0164-7.

Guarino, Domenico and Alain Destexhe (2023). "Analyzing neuromodulation dynamics with the Adaptive Exponential Integrate-and-Fire model". To be published.

Izhikevich, E.M. (2004). "Which model to use for cortical spiking neurons?" In: *IEEE Transactions on Neural Networks* 15.5, pp. 1063–1070. DOI: 10.1109/TNN.2004.832719.

Jones, Edward G (1985). "Principles of thalamic organization". In: *The thalamus*. Springer, pp. 85–149.

Kandel, Eric R., James H. Schwartz, and Thomas M. Jessell, eds. (1991). *Principles of Neural Science*. Third. New York: Elsevier.

Kuhn, Alexandre, Ad Aertsen, and Stefan Rotter (2004). "Neuronal Integration of Synaptic Input in the Fluctuation-Driven Regime". In: *Journal of Neuroscience* 24.10, pp. 2345–2356. ISSN: 0270-6474. DOI: 10.1523/JNEUROSCI.3349-03.2004. eprint: https://www.jneurosci.org/content/24/10/2345.full.pdf. URL: https://www.jneurosci.org/content/24/10/2345.

Lee, Seung-Chan et al. (2014). "Two Functionally Distinct Networks of Gap Junction-Coupled Inhibitory Neurons in the Thalamic Reticular Nucleus". In: *Journal of Neuroscience* 34.39, pp. 13170–13182. ISSN: 0270-6474. DOI: 10.1523/JNEUROSCI.0562-14.2014. eprint: https://www.jneurosci.org/content/34/39/13170.full.pdf. URL: https://www.jneurosci.org/content/34/39/13170.

McCormick, D. and D Prince (1986). "Acetylcholine induces burst firing in thalamic reticular neurones by activating a potassium conductance". In: *Nature* 319, pp. 402–405. URL: https://doi.org/10.1038/319402a0.

McCormick, David A, Matthew J McGinley, and David B Salkoff (2015). "Brain state dependent activity in the cortex and thalamus". In: *Current Opinion in Neurobiology* 31. SI: Brain rhythms

and dynamic coordination, pp. 133–140. ISSN: 0959-4388. DOI: https://doi.org/10.1016/j.conb.2014.10.003. URL: https://www.sciencedirect.com/science/article/pii/S0959438814002037.

Mitchell, Anna S. et al. (2014). "Advances in Understanding Mechanisms of Thalamic Relays in Cognition and Behavior". In: *Journal of Neuroscience* 34.46, pp. 15340–15346. ISSN: 0270-6474. DOI: 10.1523/JNEUROSCI.3289-14.2014. eprint: https://www.jneurosci.org/content/34/46/15340.full.pdf. URL: https://www.jneurosci.org/content/34/46/15340.

Pinault, Didier and Martin Deschênes (1998). "Projection and innervation patterns of individual thalamic reticular axons in the thalamus of the adult rat: A three-dimensional, graphic, and morphometric analysis". In: *Journal of Comparative Neurology* 391.2, pp. 180–203. DOI: https://doi.org/10.1002/(SICI)1096-9861(19980209)391:2<180::AID-CNE3>3.0.CO;2-Z. eprint: https://onlinelibrary.wiley.com/doi/pdf/10.1002/%28SICI%291096-9861%2819980209%29391%3A2%3C180%3A%3AAID-CNE3%3E3.0.CO%3B2-Z. URL: https://onlinelibrary.wiley.com/doi/abs/10.1002/%28SICI%291096-9861%2819980209%29391%3A2%3C180%3A%3AAID-CNE3%3E3.0.CO%3B2-Z.

Ramcharan, Eion J., James W. Gnadt, and S. Murray Sherman (2000). "Burst and tonic firing in thalamic cells of unanesthetized, behaving monkeys". In: *Visual Neuroscience* 17.1, pp. 55–62. DOI: 10.1017/S0952523800171056.

Rose, Jerzy E and Clinton N Woolsey (1949). "Organization of the mammalian thalamus and its relationships to the cerebral cortex". In: *Electroencephalography and clinical neurophysiology* 1.1-4, pp. 391–404.

Rosenstein, Michael T., James J. Collins, and Carlo J. De Luca (1993). "A practical method for calculating largest Lyapunov exponents from small data sets". In: *Physica D: Nonlinear Phenomena* 65.1, pp. 117–134. ISSN: 0167-2789. DOI: https://doi.org/10.1016/0167-2789(93)90009-P. URL: https://www.sciencedirect.com/science/article/pii/016727899390009P.

Sanz-Leon, Paula et al. (2015). "Mathematical framework for large-scale brain network modeling in The Virtual Brain". In: *NeuroImage* 111, pp. 385–430. ISSN: 1053-8119. DOI: https://doi.org/10.1016/j.neuroimage.2015.01.002. URL: https://www.sciencedirect.com/science/article/pii/S1053811915000051.

Schreiner, Thomas et al. (2022). "The human thalamus orchestrates neocortical oscillations during NREM sleep". In: *Nat Commun* 13. DOI: https://doi.org/10.1038/s41467-022-32840-w.

Sherman, Murray and Rainer Guillery (Jan. 2009). *Exploring the Thalamus and Its Role in Cortical Function*. ISBN: 9780262316231. DOI: 10.7551/mitpress/2940.001.0001.

Sherman, Murray S. and Christof Koch (2004). "The control of retinogeniculate transmission in the mammalian lateral geniculate nucleus". In: *Experimental Brain Research* 63, pp. 1–20. URL: https://api.semanticscholar.org/CorpusID:3220019.

Shu, Yousheng and David A. McCormick (2002). "Inhibitory interactions between ferret thalamic reticular neurons." In: *Journal of neurophysiology* 87 5, pp. 2571–6. URL: https://api.semanticscholar.org/CorpusID:18553357.

Steriade, M, M Deschênes, et al. (1985). "Abolition of spindle oscillations in thalamic neurons disconnected from nucleus reticularis thalami". In: *J Neurophysiol.* 54(6), pp. 1473–1497. DOI: https://doi.org/10.1152/jn.1985.54.6.1473.

Steriade, M., Igor Timofeev, and F. Grenier (May 2001). "Natural Waking and Sleep States: A View From Inside Neocortical Neurons". In: *J Neurophysiol* 85, pp. 1969–85. DOI: 10.1152/jn.2001.85.5.1969.

Steriade, Mircea (2003). *Neuronal Substrates of Sleep and Epilepsy*. Cambridge University Press. DOI: 10.1017/CBO9780511541711.

Stimberg, Marcel, Romain Brette, and Dan FM Goodman (Aug. 2019). "Brian 2, an intuitive and efficient neural simulator". In: *eLife* 8. Ed. by Frances K Skinner, e47314. ISSN: 2050-084X. DOI: 10.7554/eLife.47314.

Touboul, Jonathan and Romain Brette (Dec. 2008). "Dynamics and bifurcations of the adaptive exponential integrate-and-fire model". In: *Biological cybernetics* 99, pp. 319–34. DOI: 10.1007/s00422-008-0267-4.

Victor, Jonathan D. et al. (2011). "Mean-field modeling of thalamocortical dynamics and a model-driven approach to EEG analysis". In: *Proceedings of the National Academy of Sciences* 108.supplement_3, pp. 15631–15638. DOI: 10.1073/pnas.1012168108. eprint: https://www.pnas.org/doi/pdf/10.1073/pnas.1012168108. URL: https://www.pnas.org/doi/abs/10.1073/pnas.1012168108.

Vogels, Tim P. and L. F. Abbott (2005). "Signal Propagation and Logic Gating in Networks of Integrate-and-Fire Neurons". In: *Journal of Neuroscience* 25.46, pp. 10786–10795. ISSN: 0270-6474. DOI: 10.1523/JNEUROSCI.3508-05.2005. eprint: https://www.jneurosci.org/content/25/46/10786.full.pdf. URL: https://www.jneurosci.org/content/25/46/10786.

Wang, Chaoming, Shangyang Li, and Si Wu (2021). "Analysis of the Neuron Dynamics in Thalamic Reticular Nucleus by a Reduced Model". In: *Frontiers in Computational Neuroscience* 15. ISSN: 1662-5188. DOI: 10.3389/fncom.2021.764153. URL: https://www.frontiersin.org/articles/10.3389/fncom.2021.764153.

Wimmer, Ralf D. et al. (2015). "Thalamic control of sensory selection in divided attention". In: *Nature* 526.705. DOI: 10.1038/nature15398. URL: https://doi.org/10.1038/nature15398.

Wolfart, Jakob et al. (2005). "Synaptic background activity controls spike transfer from thalamus to cortex". In: *Nature Neuroscience* 8, pp. 1760–1767. URL: https://api.semanticscholar.org/CorpusID:1352493.

Zerlaut, Yann et al. (May 2016). "Heterogeneous firing rate response of mice layer V pyramidal neurons in the fluctuation-driven regime". In: *The Journal of Physiology* 594. DOI: 10.1113/JP272317.